



Maize (*Zea mays* L.) Nucleoskeletal Proteins Regulate Nuclear Envelope Remodeling and Function in Stomatal Complex Development and Pollen Viability

OPEN ACCESS

Joseph F. McKenna^{1††}, Hardeep K. Gumber^{2††}, Zachary M. Turpin², Alexis M. Jalovec², Andre C. Kartick², Katja Graumann^{3*} and Hank W. Bass^{2*†}

Edited by:

Christopher J. Staiger,
Purdue University, United States

Reviewed by:

Motoki Tominaga,
Waseda University, Japan
Viktor Zarsky,
Charles University, Czechia

*Correspondence:

Katja Graumann
kgraumann@brookes.ac.uk
Hank W. Bass
bass@bio.fsu.edu

†ORCID:

Joseph F. McKenna
orcid.org/0000-0003-4838-6048
Hardeep K. Gumber
orcid.org/0000-0001-5250-7207
Hank W. Bass
orcid.org/0000-0003-0522-0881

†These authors have contributed
equally to this work and share first
authorship

Specialty section:

This article was submitted to
Plant Cell Biology,
a section of the journal
Frontiers in Plant Science

Received: 22 December 2020

Accepted: 27 January 2021

Published: 17 February 2021

Citation:

McKenna JF, Gumber HK,
Turpin ZM, Jalovec AM, Kartick AC,
Graumann K and Bass HW (2021)
Maize (*Zea mays* L.) Nucleoskeletal
Proteins Regulate Nuclear Envelope
Remodeling and Function in Stomatal
Complex Development and Pollen
Viability. *Front. Plant Sci.* 12:645218.
doi: 10.3389/fpls.2021.645218

¹ School of Life Sciences, University of Warwick, Coventry, United Kingdom, ² Department of Biological Science, Florida State University, Tallahassee, FL, United States, ³ Department of Biological and Medical Sciences, Oxford Brookes University, Oxford, United Kingdom

In eukaryotes, the nuclear envelope (NE) encloses chromatin and separates it from the rest of the cell. The Linker of Nucleoskeleton and Cytoskeleton (LINC) complex physically bridges across the NE, linking nuclear and cytoplasmic components. In plants, these LINC complexes are beginning to be ascribed roles in cellular and nuclear functions, including chromatin organization, regulation of nuclei shape and movement, and cell division. Homologs of core LINC components, KASH and SUN proteins, have previously been identified in maize. Here, we characterized the presumed LINC-associated maize nucleoskeletal proteins NCH1 and NCH2, homologous to members of the plant NMCP/CRWN family, and MKAKU41, homologous to AtKAKU4. All three proteins localized to the nuclear periphery when transiently and heterologously expressed as fluorescent protein fusions in *Nicotiana benthamiana*. Overexpression of MKAKU41 caused dramatic changes in the organization of the nuclear periphery, including nuclear invaginations that stained positive for non-nucleoplasmic markers of the inner and outer NE membranes, and the ER. The severity of these invaginations was altered by changes in LINC connections and the actin cytoskeleton. In maize, MKAKU41 appeared to share genetic functions with other LINC components, including control of nuclei shape, stomatal complex development, and pollen viability. Overall, our data show that NCH1, NCH2, and MKAKU41 have characteristic properties of LINC-associated plant nucleoskeletal proteins, including interactions with NE components suggestive of functions at the nuclear periphery that impact the overall nuclear architecture.

Keywords: nuclear envelope, maize, lamin, nucleoskeleton, KAKU4, nucleus, peripheral nucleoplasm

INTRODUCTION

In plant cells, as with all eukaryotes, the nucleus is a conspicuous and characteristic organelle, housing the DNA (reviewed by Meier et al., 2017). The nucleus itself is a dynamic structure, organized largely by its enclosing membrane system - the nuclear envelope (NE). The NE is a double-membraned structure composed of an outer nuclear membrane (ONM) and an inner

nuclear membrane (INM) connected at nuclear pores (reviewed by Hetzer, 2010; Graumann and Evans, 2017). The functional properties of the NE are mediated by protein complexes linked to myriad cellular and nuclear processes, including cell division and gene expression (Kim et al., 2015; Meier et al., 2017; De Magistris and Antonin, 2018; Pradillo et al., 2019). A major conserved NE complex is the linker of nucleoskeleton and cytoskeleton (LINC) complex (Crisp et al., 2006), known for its involvement in processes such as the maintenance of nuclear architecture and mechanical structures, signaling, nuclear motility, and nuclear positioning (reviewed by Rothballer and Kutay, 2013; Chang et al., 2015; Tamura et al., 2015; Pradillo et al., 2019; Starr, 2019). Well beyond the historically recognized role of compartmentalization, NE investigations increasingly address how the NE contributes to both general and specialized functions in plant growth and development. The underlying molecular mechanisms coordinating and regulating these fundamental NE processes remain, however, largely unknown.

The hallmark of LINC complexes is their ability to form direct connections bridging the cytoplasm and the nucleoplasm. This is accomplished by a core complex of two groups of proteins, residing on the two separate membranes of the NE. The INM houses the Sad1/UNC84 homology (SUN) domain proteins and the ONM houses the Klarsicht/ANC-1/Syne homology (KASH) proteins (Hagan and Yanagida, 1995; Malone et al., 1999; Starr, 2002; Murphy et al., 2010). As a group, the KASH proteins are numerous and diverse, reflecting their various cytoplasmic binding partners, such as cytoskeletal and motor proteins (Starr and Fridolfsson, 2010; Luxton and Starr, 2014; Kim et al., 2015; Evans and Graumann, 2018; Starr, 2019). In contrast, the SUN-domain proteins are less diverse but still exhibit interactions with multiple components of the nucleoplasm, such as nucleoskeletal components and chromatin proteins (Haque et al., 2006; Janin et al., 2017). While cytoskeletal components of LINC complexes and the SUN proteins appear conserved in eukaryotes, plants have evolved unique KASH proteins and nucleoskeletal components. Plant nucleoskeletal components, while lacking sequence homology, share many of the animal lamin features, including interactions with the NE and their ability to impact chromatin structure and gene expression (Masuda et al., 1997; Dittmer et al., 2007; Wang et al., 2013; Ciska and Moreno Díaz de la Espina, 2014; Goto et al., 2014; Zhao et al., 2016; Guo et al., 2017; Choi et al., 2019; Ciska et al., 2019; Hu et al., 2019; Sakamoto, 2020).

Plant nucleoskeletal proteins that interact directly or indirectly with the NE fall into two families of proteins. One family, the Nuclear Matrix Constituent Proteins/Crowded Nuclei (NMCP/CRWN) proteins, is found in plants with members encoded by the NMCP genes in carrot (Masuda et al., 1997), CRWN genes in Arabidopsis (Dittmer et al., 2007), and NCH genes in maize (Gumber et al., 2019a). The other family is also found in plants and encoded by the AtKAKU4 gene in Arabidopsis (Goto et al., 2014) and the MKAKU41 and MKAKU42 genes in maize (Gumber et al., 2019a). Here we refer to these two gene or protein families generally as CRWN and KAKU4.

In Arabidopsis, CRWN1 is located primarily at the nuclear periphery and interacts with SUN-domain proteins (Dittmer et al., 2007; Graumann, 2014). CRWN proteins have been implicated in the regulation of nuclear shape, nuclear size, chromatin organization, regulation of gene expression, and nuclear body formation in plants (reviewed in Sakamoto, 2020). KAKU4 was shown to interact with CRWN1 by yeast two-hybrid analysis, supporting their cooperation in the form and function of a plant nucleoskeletal system (Goto et al., 2014). Fluorescent protein fusions driven by native promoter expression and electron microscopy showed that KAKU4 is localized to the inner nuclear membrane. Interestingly, when high-expression stable lines were selected or high-expression transient transformation was performed, KAKU4 appeared to induce nuclear invaginations, which increased significantly when co-expressed with CRWN1 (Goto et al., 2014).

Together, the CRWN and KAKU proteins are known to affect phenotypes in eudicots, yet their roles in crop species are less well understood. Two maize CRWN homologs are known; NCH1 which is most closely related to AtCRWN1-3, and NCH2 which is most closely related to AtCRWN4. Maize MKAKU41 homologs are encoded by *MKAKU41* and *MKAKU42* (Gumber et al., 2019a). To investigate the functional conservation of these presumed nucleoskeletal proteins in maize, we characterized *NCH1* and *NCH2* and *MKAKU4* using cytological or genetic approaches.

RESULTS

Maize NCH1, NCH2, and MKAKU41 Localized to the Nucleus, Primarily at the Nuclear Periphery

In order to determine the cellular localization of the maize CRWN homologs NCH1, NCH2, and the KAKU4 homolog MKAKU41, we produced gene constructs with the protein coding region fused to either GFP or mCherry at the N-terminus. We then expressed these constructs transiently in *N. benthamiana* leaf tissue. All three constructs localized to the nuclear periphery with MKAKU41 also exhibiting internal structures as shown in **Figure 1** for nuclei counterstained with DAPI. In order to confirm that NCH1 and NCH2 were localized at the nuclear periphery, we performed co-expression of NCH1 or NCH2 with AtCRWN1 (**Supplementary Figure 1**). The colocalization of NCH with CRWN confirmed that NCH1 and NCH2 did localize to the nuclear periphery when transiently expressed in *N. benthamiana*. Interestingly, MKAKU41 showed nuclear envelope labeling and inner nucleus labeling in most cells, including membrane invaginations (**Figure 1A**, white arrowheads), as has been described for Arabidopsis KAKU4 when expressed under the control of the 35S promoter (Goto et al., 2014). These included internal structures and circular ring-like invaginations within the nucleus. The structures labeled with MKAKU41 colocalized with brighter DAPI staining regions, implying that MKAKU41 may associate with heterochromatin. The ring-like invaginations lacked internal DAPI staining and therefore appeared devoid of typical nucleoplasmic chromatin.

Interestingly, the CRWN1 homolog NCH1 alone also caused these aberrant-looking intranuclear structures (**Figure 1A**, white arrow), although to a lesser extent than MKAKU41. However, NCH2, a CRWN4 homolog (Ciska et al., 2019), did not induce ring-like invaginations. The NCH1 and NCH2 also displayed different mobility proportions at the nuclear periphery (Figure 1B and **Supplementary Figures 1B–F**) as determined by Fluorescence Recovery After Photobleaching (FRAP). NCH2 was significantly less mobile (16% mobile fraction) than NCH1 (49% mobility) indicating that they might interact with different protein complexes or structures. The lower mobility of NCH2 compared to NCH1 is consistent with its reduced capacity to remodel the nuclear envelope membrane and cause invaginations (**Figure 1**). The large immobile fraction of NCH2, but not NCH1, was comparable to that of AtCRWN1 (Graumann, 2014).

It has been demonstrated that the degree of nuclear invagination and deformation is dependent on the expression level of KAKU4 in *A. thaliana* (Goto et al., 2014). We therefore asked if this causal relationship was conserved in the maize genes, MKAKU41, NCH1, and NCH2, using the dose-response transient expression assays summarized in **Figure 2**. We infiltrated *N. benthamiana* with three different concentrations of Agrobacterium, OD 0.01, 0.05, or 0.1, and then classified live-imaged nuclei ($N \geq 30$ per condition) into one of three previously described nuclear periphery cytological image patterns (Goto et al., 2014): type I for normal nuclear periphery localization, type II for minor invaginations or inclusions in the nucleus, and type III for major invaginations and deformation of the nucleus. This classification assisted with a comparative analysis of the severity of changes in nuclear morphology across the various experiments used throughout this study. Increasing the infiltration concentration of NCH1 resulted in progressively increased nuclear deformation illustrated by type II pattern increases and the appearance of type III at the highest transfection dose (**Figure 2A**). NCH2 also showed a transfection dose-dependent increase in nuclear aberration coupled to type II increases, but less so and without any type III nuclei even at the highest dose (**Figure 2B**). For MKAKU41, increasing the transfecting plasmid concentration led from most nuclei just showing peripheral localization initially to slightly under half showing type III patterns with severe invaginations seen at the highest concentration (**Figure 2C**). We interpret these results as establishing that because all three of the proteins tested showed they could cause dose-dependent increases in severity of nuclear deformation patterns, they can all be considered to be part of the same process, one needed to properly organize a nuclear periphery compartment within interphase nuclei.

Co-expression of NCH1 or NCH2 With MKAKU41 Showed a Synergistic Effect on Invagination and Nuclear Deformation Phenotypes

The Arabidopsis CRWN1 and KAKU4 have previously been shown to result in increased nuclear deformation and invaginations when co-expressed (Goto et al., 2014). In order to determine whether the maize homologs similarly affect the

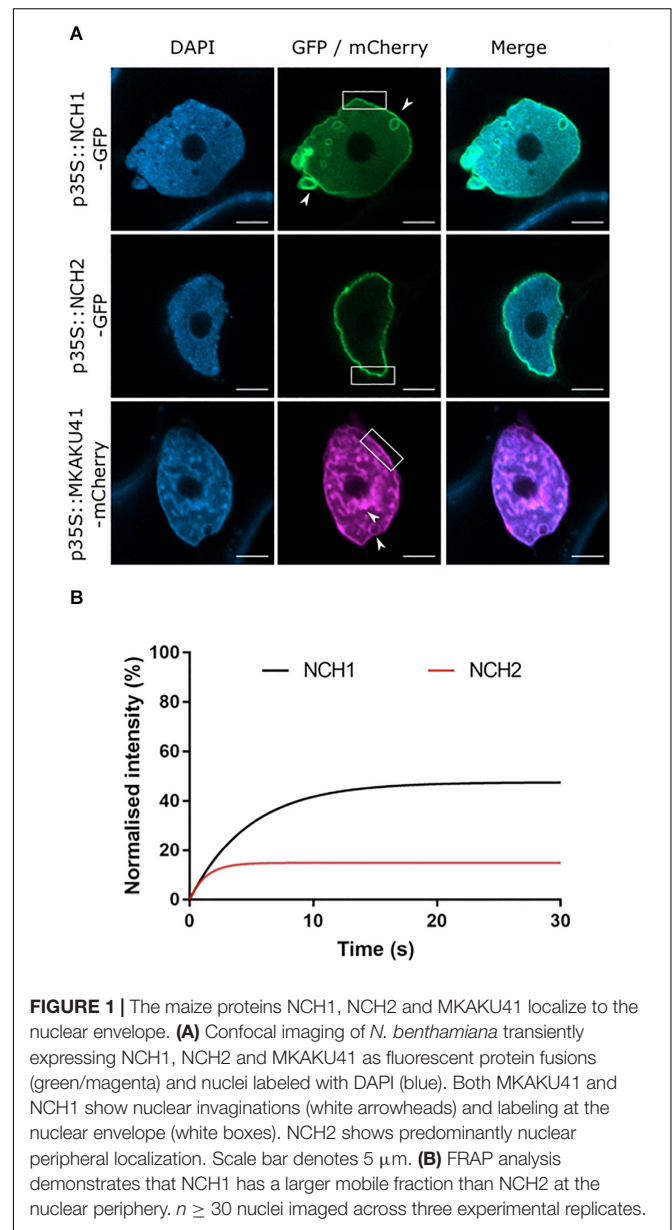
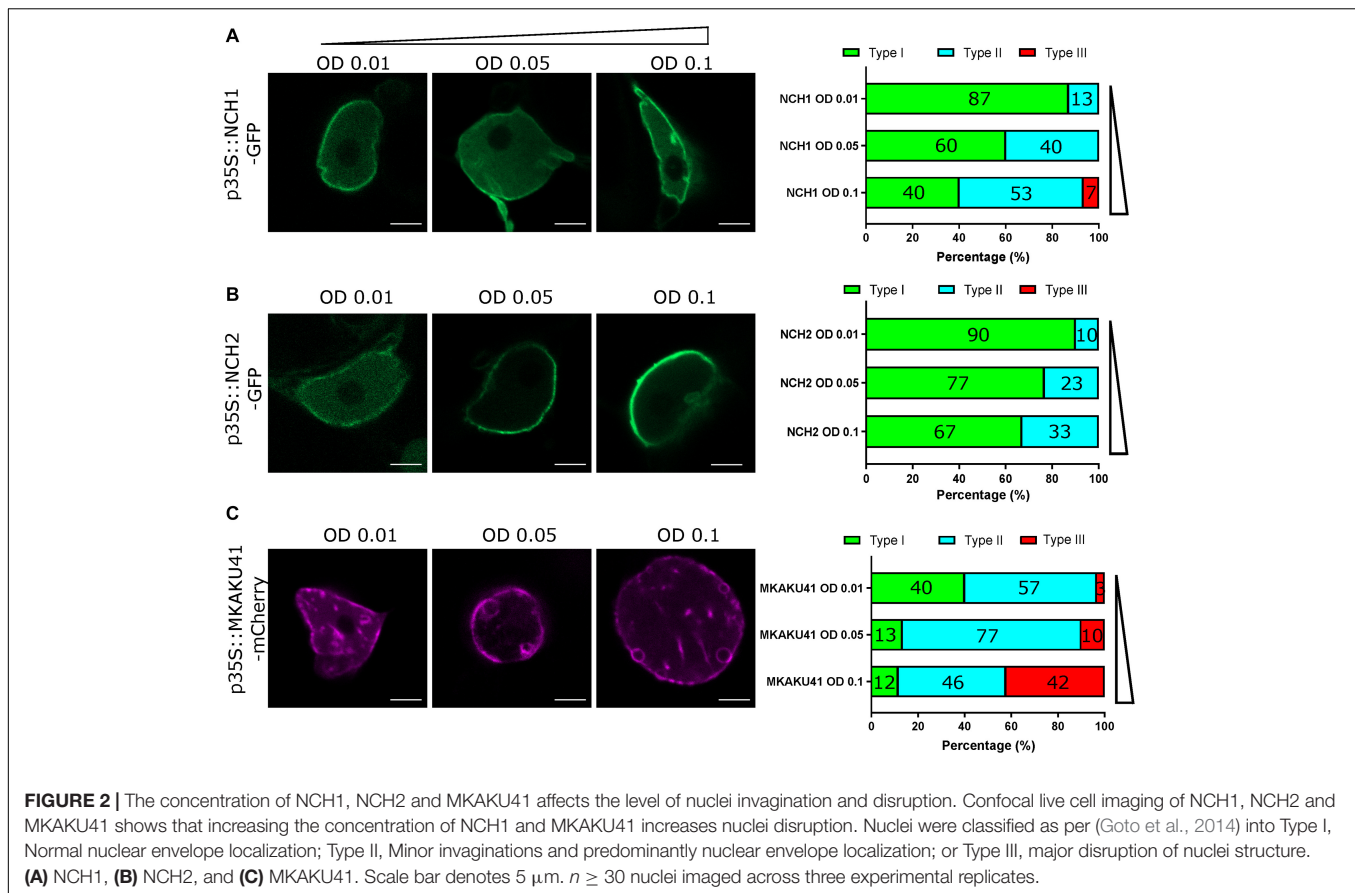


FIGURE 1 | The maize proteins NCH1, NCH2 and MKAKU41 localize to the nuclear envelope. **(A)** Confocal imaging of *N. benthamiana* transiently expressing NCH1, NCH2 and MKAKU41 as fluorescent protein fusions (green/magenta) and nuclei labeled with DAPI (blue). Both MKAKU41 and NCH1 show nuclear invaginations (white arrowheads) and labeling at the nuclear envelope (white boxes). NCH2 shows predominantly nuclear peripheral localization. Scale bar denotes 5 μm. **(B)** FRAP analysis demonstrates that NCH1 has a larger mobile fraction than NCH2 at the nuclear periphery. $n \geq 30$ nuclei imaged across three experimental replicates.

nuclear organization pathway, we co-expressed MKAKU41 with either NCH1 or NCH2 as presented in **Figure 3**. Upon co-expression, the nuclear invaginations and deformations were substantially enhanced compared to single-expression (**Figure 3A**). Quantifying the most severe phenotype (type III), we observed that NCH1 alone exhibited 7% and MKAKU41 alone exhibited 42%. However, the combination of NCH1 and MKAKU41 exhibited 88% type III, well beyond the combined value of 49%, and thus synergistic for this measurement. Similarly, the NCH2 and MKAKU41 co-expression reached a level of 66% type III nuclei, considerably more than 42% sum of the single-expressed levels. Therefore, NCH proteins appeared to act cooperatively with MKAKU41 to affect nuclear periphery organization as judged by changes in their localization patterns. This cumulative effect on nuclear structure suggests



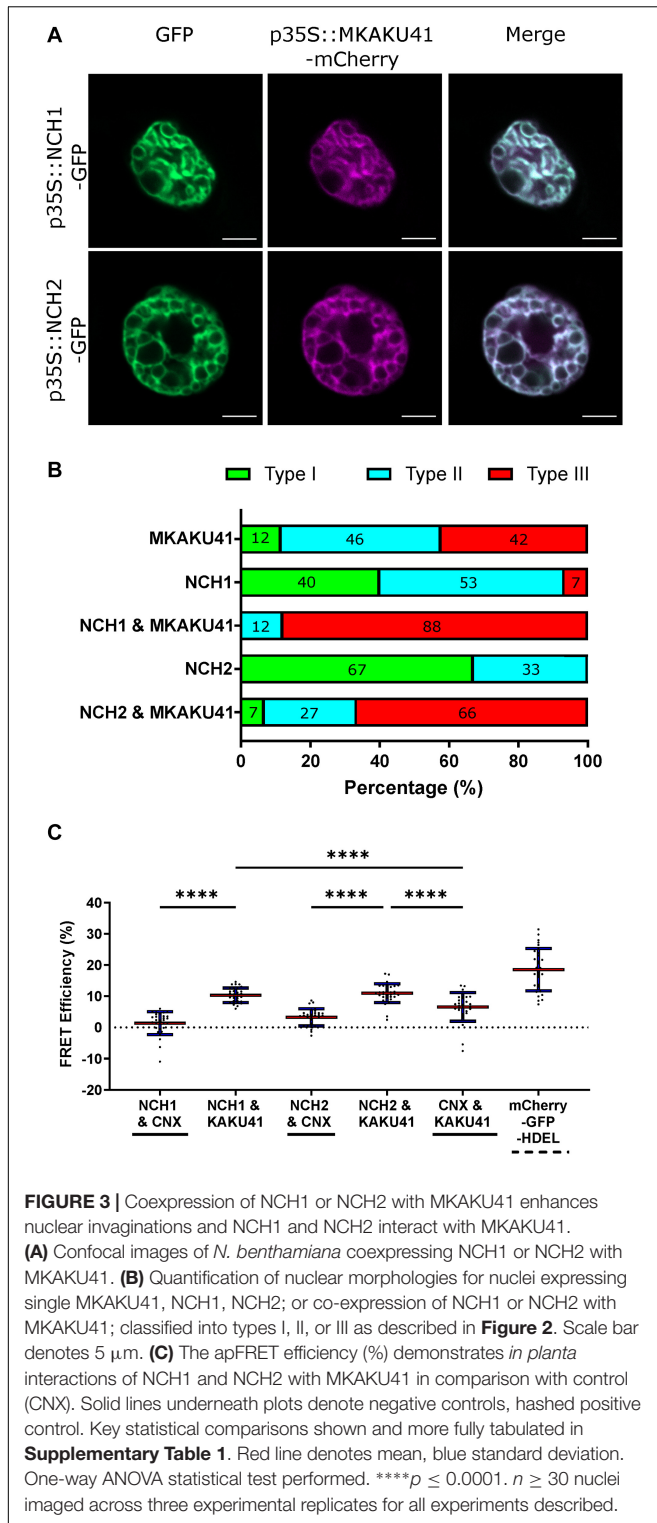
that NCH1/NCH2 and MKAKU41 may act in the same protein complex. We tested this idea by checking for evidence of interaction between NCH and MKAKU41 *in planta* using acceptor photobleaching fluorescence resonance energy transfer (apFRET). A significant rise in FRET efficiencies would indicate interactions and such was measured when NCH1 and NCH2 were co-expressed with MKAKU41, compared to a non-interacting control, calnexin (Figure 3C). Internal control FRET efficiency% values were very low, as expected for non-bleached controls (Supplementary Table 1). This demonstrated that NCH1 and NCH2 can interact with MKAKU41, and is consistent with their synergistic effect on levels of nuclear deformations. This observation is similar to that observed for Arabidopsis homologs using yeast two-hybrid system and plant expression (Goto et al., 2014). Importantly, our findings provide evidence from live imaging for *in planta* interactions between these proteins at the nuclear periphery.

MKAKU41 Overexpression Remodeled Other Inner and Outer Nuclear Membrane Proteins

Both AtKAKU4 and MKAKU41 cause deformation of the NE and disruption of nuclei structure when co-expressed with AtCRWN1 (Goto et al., 2014), NCH1, or NCH2 (Figure 3). To further investigate whether this involves the entire NE,

we asked whether overexpression of MKAKU41 can result in the invagination of other proteins not previously tested but known to localize to either the INM, the ONM, or the ER. For this we used AtSUN2-YFP to mark the INM, ZmMLKP1-GFP to mark the ONM, and calnexin-GFP to mark the ER membrane. Figure 4 shows that each of these markers showed normal nuclear periphery localization when expressed individually. However, upon co-expression with MKAKU41, all of these proteins appeared in aberrant intranuclear structures. Therefore, the expression of MKAKU41 appears to have caused the internalization of the entire NE, including the calnexin-GFP ER membrane marker, demonstrating that MKAKU41-induced nuclei deformations and invaginations are not limited to nucleoplasmic and INM LINC proteins.

Previously, it has been shown that AtSUN1 and AtSUN2 interact with AtCRWN1, mediated by the SUN N-terminus (Graumann, 2014) and that the deletion construct SUN2 Δ Nterm could disrupt SUN-CRWN interactions (Graumann et al., 2010; Graumann, 2014). To investigate more specifically the role of the LINC complex in producing these aberrant nuclear structures, we overexpressed SUN2 Δ Nterm as a way to abrogate CRWN-SUN binding and thereby possibly reduce the interaction of MKAKU41 with the LINC complex. Notably, SUN2-MKAKU41 co-expression resulted in mostly type III nuclei, whereas the SUN2 Δ Nterm-MKAKU41 co-expression led to less deformation, with nuclei showing mostly type II phenotype (Figure 4A).



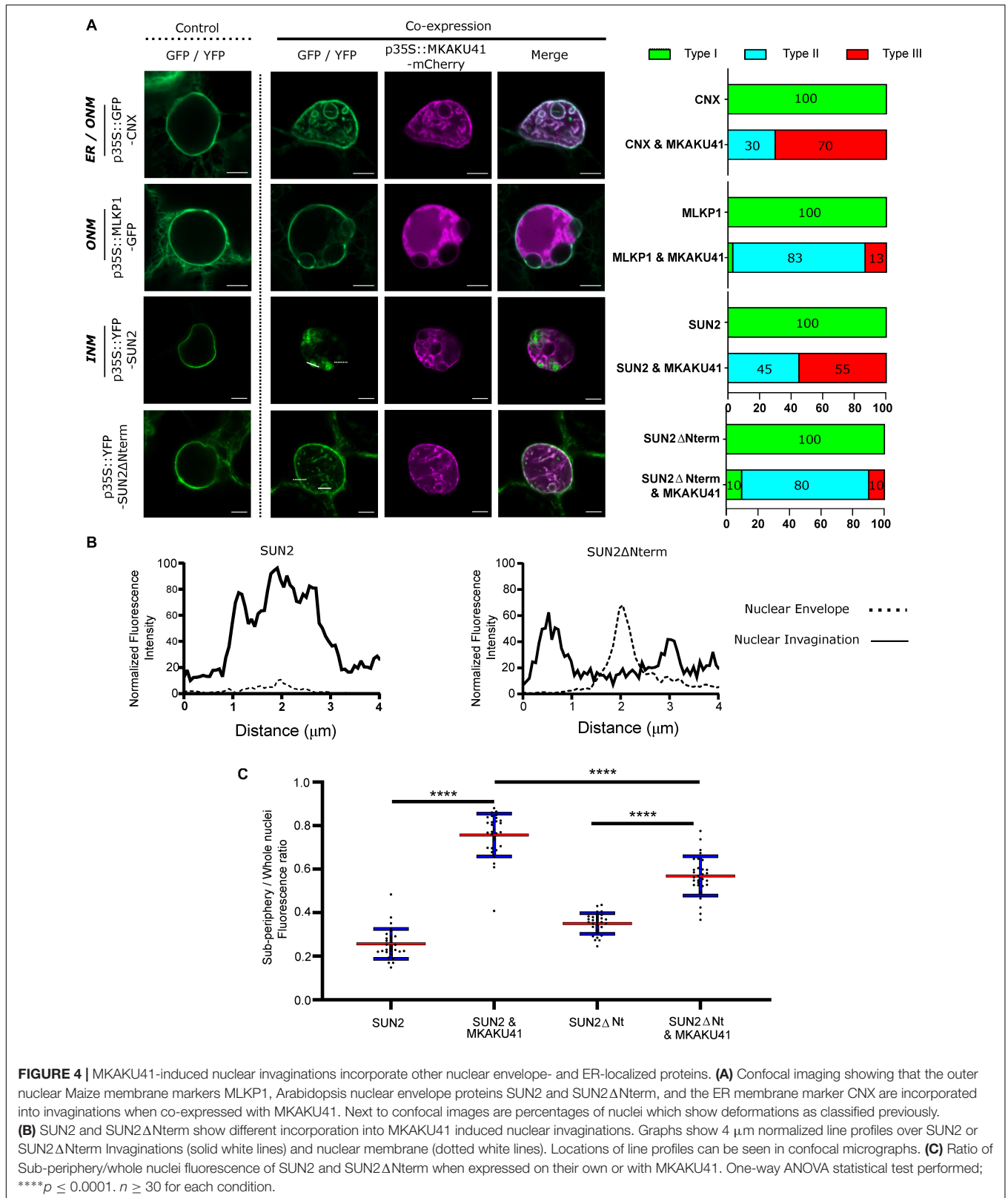
Interestingly, nuclear envelope fluorescent labeling of full-length SUN2 appeared lower than that in SUN2 Δ Nterm when co-expressed with MKAKU41 (**Figures 4A,B**). Signal intensity line profiles drawn over the nuclear invagination (**Figure 4A**, dashed line) or nuclear envelope (**Figure 4A**, solid line) regions

showed that the SUN2 full length signal was much stronger within the invaginations but lower at the nuclear envelope when compared to those from SUN2 Δ Nterm fluorescence (**Figure 4B**). We quantified the effect of co-expressed MKAKU41 on the SUN2's tendency for peripheral staining by determining the percentage of the signal in the interior versus the entire nucleus (sub-periphery/whole nucleus/, **Supplementary Figure 2**). For instance, if the signal was entirely peripheral, the percentage would be at or near zero. **Figure 4C** shows an increase in internal fluorescence for SUN2 in the SUN2 - MKAKU41 co-expression compared to SUN2 alone ($p < 0.0001$). Therefore, full length SUN2 is relocated away from the nuclear periphery when coexpressed with MKAKU41. The relative internal nuclear fluorescence also increased upon SUN2 Δ Nterm coexpression with MKAKU41 ($p < 0.001$), but to a lesser extent than for full length SUN2 ($p < 0.001$). These observations implicate the LINC complex and more specifically the nucleoplasmic N-terminal domain of the NE protein, SUN2, in the formation of aberrant MKAKU41-dependent intranuclear structures.

Impairing Nuclear Actin Anchoring Enhances Nuclear Invaginations

In addition to the SUN2 NE protein which spans the INM and has direct contact with the nucleoplasm, we also examined an ONM maker, MLKS2, and its ARM domain deletion derivative previously shown to be impaired for actin binding (Gumber et al., 2019b). Upon co-expression with MKAKU41, the ONM marker MLKS2 also appeared in intranuclear invagination-like structures as shown in **Figure 5A**. Upon co-expression of MKAKU4 and MLKS2 Δ ARM, nuclear deformations and invaginations were observed (**Figure 5A**) and found to much more severe and abundant (**Figure 5B**) compared to those from co-expression of MKAKU4 and the full length MLKS2. Therefore, the ONM KASH protein MLKS2 is brought moved to intranuclear structures by MKAKU41 co-expression, and loss of the actin-interacting ARM domain exacerbates the situation and implicates cytoplasmic F-actin in NE and nuclear periphery remodeling.

In order to further probe the interaction between peri-nuclear actin and MKAKU41-induced nuclear deformations, we used Latrunculin-B (LatB) to depolymerize the actin cytoskeleton as described previously (McKenna et al., 2019). **Figure 5C** shows that upon expression of MKAKU41 at a moderate level (O.D. 0.05), LatB depolymerization of the actin cytoskeleton resulted in a statistically significant increase in the number of invaginations ($p \leq 0.001$). While this trend existed at lower (O.D. 0.01) and higher transfection concentrations (O.D. 0.10), it was not statistically significant. To further explore the connection between the actin cytoskeleton and MKAKU41 induced nuclear deformations, we examined the interior versus peripheral signal ratios (**Supplementary Figure 2**) and found that actin depolymerization quantitatively shifted the INM NE marker, LBR, toward increased interior signal (**Figure 5D**). This same effect was seen and found to be statistically significant for two concentrations of MKAKU41 infiltration (O.D. 0.01) ($p = 0.01$) and 0.05 ($p = 0.05$). This demonstrates that at the moderate transfection concentration of (O.D. 0.05), actin depolymerization



with LatB increases the internalization of peripheral markers. These findings corroborate those from the MLKS2ΔARM

experiments in that they implicate F-actin as a possible factor that can provide an opposing force or counterbalance to

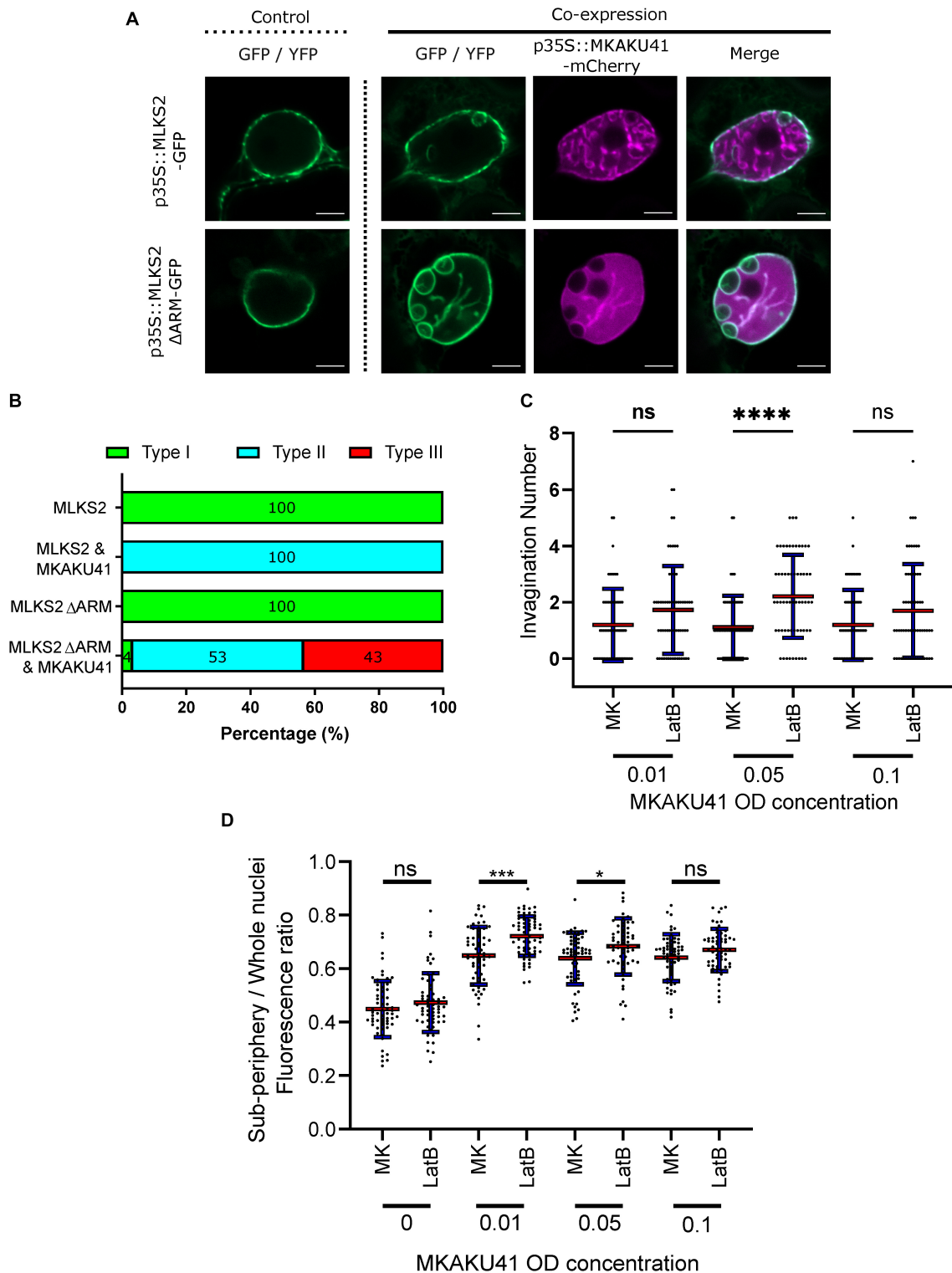


FIGURE 5 | Nuclear actin anchoring is important for regulating nuclei deformations upon MKAKU41 overexpression. **(A)** Confocal live cell imaging of MLKS2 and MLKS2ΔARM single and co-expression with MKAKU41. **(B)** All nuclei imaged were categorized on the level of disruption as described previously. **(C)** Number of nuclei invaginations at different MKAKU41 expression levels with actin depolymerized (LatB). **(D)** Sub-periphery/whole nuclei fluorescence ratio from nuclei expressing different levels of MKAKU41 (MK, from 0 to 0.1) with and without actin depolymerization (LatB). Nuclei were imaged with the NE marker LBR-GFP. Scale bar denotes 5 μm. $n \geq 30$ nuclei imaged across three experimental replicates for panels **A** and **B**. For Panels **C** and **D**, one-way ANOVA statistical test performed; ns $p \geq 0.05$, * $p \leq 0.05$, *** $p \leq 0.001$, and **** $p \leq 0.0001$. $n \geq 60$ across three biological replicates.

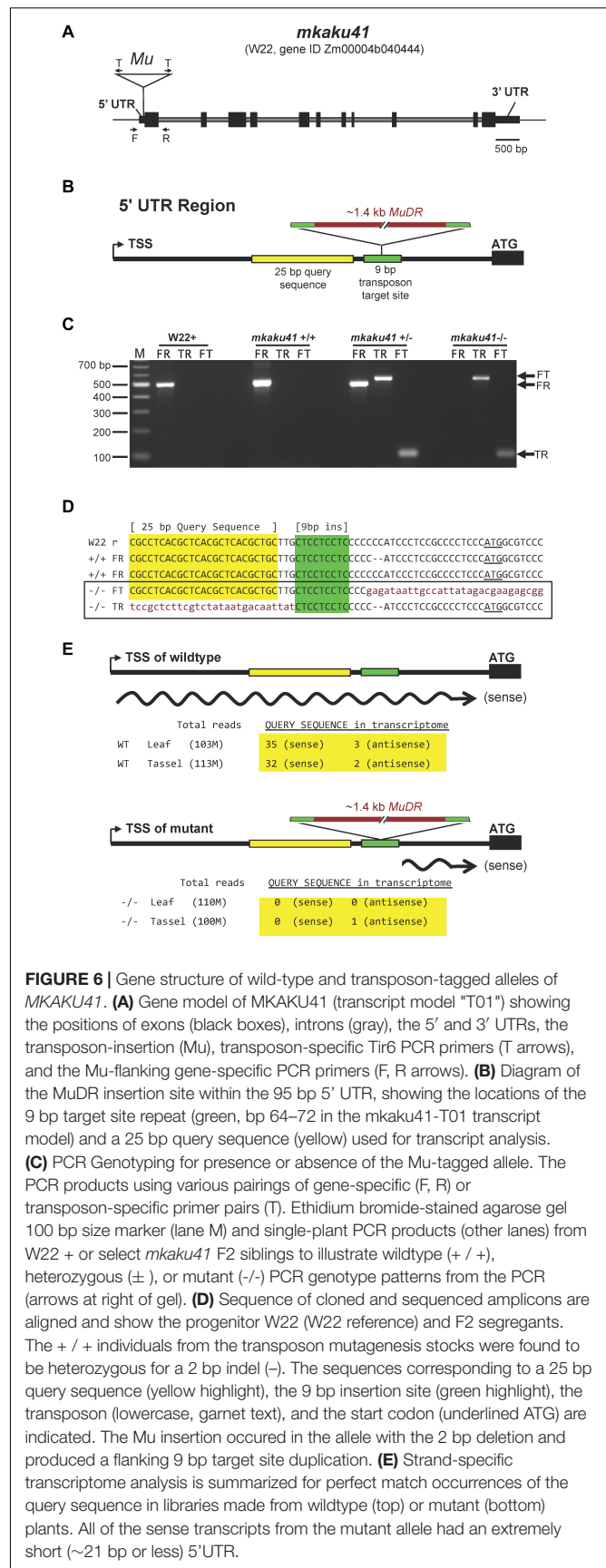
nucleoskeletal proteins which can invaginate the NE and create inclusion bodies in a concentration-dependent manner.

Transposon Disruption of the MKAKU41 Gene Co-segregates With Phenotypic Effects on Nuclear Shape and Development

Having seen that overexpression of maize MKAKU41 in a eudicot species resulted in nuclear architecture disruption and severe nuclear envelope misplacement, we wanted to examine the role of this gene in its native genetic background, maize. From the UniformMu transposon mutagenesis project, we found and characterized a Mutator-tagged allele of *MKAKU41*, allowing for a genetic examination of the biological consequences of gene disruption in maize.

The transposon-tagged allele, here designated *mkaku41*, and its wild-type counterpart, *MKAKU41*, are shown in **Figure 6**. The wild-type *MKAKU41* gene (Zm00004b040444) from the color-converted W22 inbred is annotated as being associated with three transcript models. The gene structure for transcript model T01 (**Figure 6A**) spans 7.9 kb, with 11 exons producing an mRNA with a single large ORF predicted to encode a protein of 579 AA. The transposon insertion site (mu1005806) is located in the 5' UTR (**Figure 6B**). The transposon insertion allele was characterized by genomic PCR analysis (**Figure 6C**) using various combinations of primers that were flanking the insertion site, and were gene-specific and *Mutator*-specific (**Figure 6A**, primers F, T, R). These PCR products were visualized (**Figure 6C**) and sequenced (**Figure 6D**) from the W22 wild type progenitor (W22 +) as well as F2 individuals from families segregating for *mkaku41* (+/+, +/-, or -/-), where the "-" symbol denotes the transposon-insertion allele. These PCR primers and PCR gel products were used for plant genotyping in subsequent analyses.

By inspection of the junction sequences between the wild-type reference W22 genome and the transposon (**Figure 6D**, lower case letters), we identified the 9-bp target site duplication as CTCCTCTC (color coded green in **Figure 6**). These results confirmed that the transposon was inserted in the 5' UTR at a position 23 bp upstream of the start codon, disrupting the majority of the wild-type 95 bp 5' UTR. The location of this insertion, while not in the protein coding region of the gene, is within the first exon and its location is expected, therefore, to disrupt the expression or transcript structure of the gene. Surprisingly, from transcriptome analysis we found that the gene expression levels for MKAKU41, measured as total normalized reads across the gene model, were similar in libraries made from wildtype and mutant leaf and tassel. We mined the transcript data to investigate the effect of the transposon insertion on the 5' UTR region by searching for the presence of a unique 25 bp 5' UTR sequence located just upstream of the mapped insertion site (**Figures 6D,E**, "Query sequence" highlighted in yellow). We found a total of 70 matches to our 25 bp query sequence in our transcriptome, which was sequenced at a depth of over 100 M reads per tissue-genotype combination (**Figure 6E**). All 70 occurrences of the query sequence were from the wildtype libraries except for one, which was on the reverse strand relative



to the gene (**Figure 6E**). These results indicate that the 5' UTR was indeed disrupted in the mutant plants. In addition to this detailed analysis of MKAKU41, some differentially expressed genes (**Supplementary Table 2**) were observed in mutant versus wild-type leaf and meiotic-enriched whole tassel, but gene ontology analysis did not reveal any clear and reproducible enrichments that differed from those of randomized controls.

We next explored the phenotypic consequences of the *mkaku41* transposon insertion on root hair nuclei, stomatal complex, and pollen viability, as summarized in **Figure 7**. The root hair nuclei in W22 + (normal) and *mkaku41* mutant seedlings 5 days after imbibition were imaged and their shapes were analyzed (**Figures 7A–F**). The mutant nuclei were visually and quantitatively more rounded than their wildtype counterparts. The mutant nuclei had an average maximum length of 22 μm whereas their wild-type counterparts averaged 34 μm (**Figure 7G**). The mutant nuclei also exhibited a higher circularity index than the wildtype nuclei (**Figure 7H**). Both measures ($n = 50$) were statistically significant as determined using *T*-test, two-tailed with $p < 0.0001$.

Next, we analyzed two above-ground phenotypes, the appearances of stomatal complexes and pollen. In W22 + plants, a normal stomatal complex is composed of two guard cells flanked by two subsidiary cells as shown for W22 + (**Figure 7I**). In contrast, mutant plants showed irregular stomatal complexes composed of two normal-looking guard cells flanked by one or two extra and irregularly positioned subsidiary cells (arrows, **Figures 7J–N**). For the pollen phenotypes, we assayed viability and shape (**Figures 7O–R**). Using the modified Alexander's differential staining method, we found that the percent of viable pollen was dramatically reduced in the mutant, from 84 to 46%. The shape of the pollen was also affected in the mutant, where the average degree of roundness decreased from 0.93 to 0.7. Both measures ($n > 1,000$ for staining, $n = 100$ for roundness) were statistically significant as determined using a two-tailed *T*-test with $p < 0.0001$.

Taken together, these findings show that the *mkaku41* mutation was associated with multiple phenotypes including root hair nuclear shape, stomatal complex development, and pollen viability. Therefore, MKAKU41 appears to act in some of the same genetic pathways as the NE-associated LINC complex proteins such as SUN and KASH. This genetic data in maize is interesting when considered with our findings that heterologous overexpression phenotypes and actin perturbations (**Figures 1–5**) disrupt nuclear architecture and nuclear envelope organization. Taken together, all of these experiments establish biological roles for MKAKU41, NCH1, and NCH2 as nucleoskeletal proteins that regulate fundamental nuclear processes in cellular structure and function.

DISCUSSION

Regulation of nucleus size and shape is important for many fundamental cellular processes in all eukaryotes. Nuclear architecture is controlled by multiple interactions involving the NE, NE-associated complexes, and the nucleoskeleton. Here,

we characterized multiple maize nucleoskeletal proteins, which, like their animal counterparts, controlled nuclear dynamics. An overarching goal motivating this study is to establish the general rules that apply across the plant domain, an evolutionarily vast space. Toward this goal, we have utilized the tobacco transient heterologous expression assay as a powerful and versatile experimental platform for plant nuclear envelope research. In this study and previously, we have established cellular localization, protein-protein interactions, dose-response phenotypes, and live cell imaging that allows for kymographic analysis, mobility via FRAP, and interactions via AP-FRET, all of which have enabled and accelerated our understanding of grass and model crop NE biology (Gumber et al., 2019a,b).

The maize nucleoskeletal proteins examined in this study are NCH1, NCH2 and MKAKU41, each of which has one or more homologs (**Figure 1A**) in eudicot species (Gumber et al., 2019a) and all of which exhibit nuclear localization and NE enrichment in heterologous expression systems. Interaction data from this (**Figure 3C**) and prior studies further indicate that these proteins are coupled to the NE via the LINC complex. These findings, together with those from other plant species, point to the broad conservation of plant nucleoskeletal proteins across angiosperms (Goto et al., 2014; Meier et al., 2017; Ciska et al., 2019; Sakamoto, 2020). The functional conservation of these components is evidenced by previously reported cross-species functional rescue (Gumber et al., 2019b) and by the current study where we show that the maize MKAKU41 (**Figure 4**) interacts with Arabidopsis AtSUN2, causing altered nuclear localization of the Arabidopsis AtSUN2.

Multiple lines of evidence for conservation of plant LINC complexes are also seen at the organismal and phenotypic level. For instance, we (**Figure 7**) and others found that mutant phenotypes commonly include the rounding up of root hair nuclei, disruption of stomatal complex development, and effects on pollen shape and viability (Dittmer et al., 2007; Goto et al., 2014, 2020; Zhou et al., 2014; Gumber et al., 2019b; Newman-Griffis et al., 2019). The nuclear shape defects in root hairs have become a hallmark of LINC defects in plants, and as such were predicted. However, the stomatal complex and pollen shape phenotypes have not been previously observed for plant mutants of MKAKU4 genes, but they resemble to some extent those of the plant KASH mutant, *mlks2* (Gumber et al., 2019b). To gain genetic insight into these nucleoskeletal proteins in the crop species maize, we searched for transposon-disrupted alleles of MKAKU41, NCH1, and NCH2. Of these, we found that the *MKAKU41* gene was reported to have a Mutator insertion (McCarty and Meeley, 2009), described here as the first known mutant allele, *mkaku41*. The insertion site was in the 5'-UTR (**Figure 6**), a common hot-spot for Mu insertion (Zhang et al., 2020). The transcript abundance was not significantly reduced in the mutants, but the mutant allele produced an extremely truncated 5' UTR of 23 bp or less. Given that the median 5' UTR length in maize was recently determined to be 132 bp (Leppek et al., 2018), such an extremely short 5' UTR in the *mkaku41* mutants may abolish or greatly decrease the ability of the cell to utilize the native start codon for translation of the full-length protein. If the mutant 5' UTR is too short for efficient

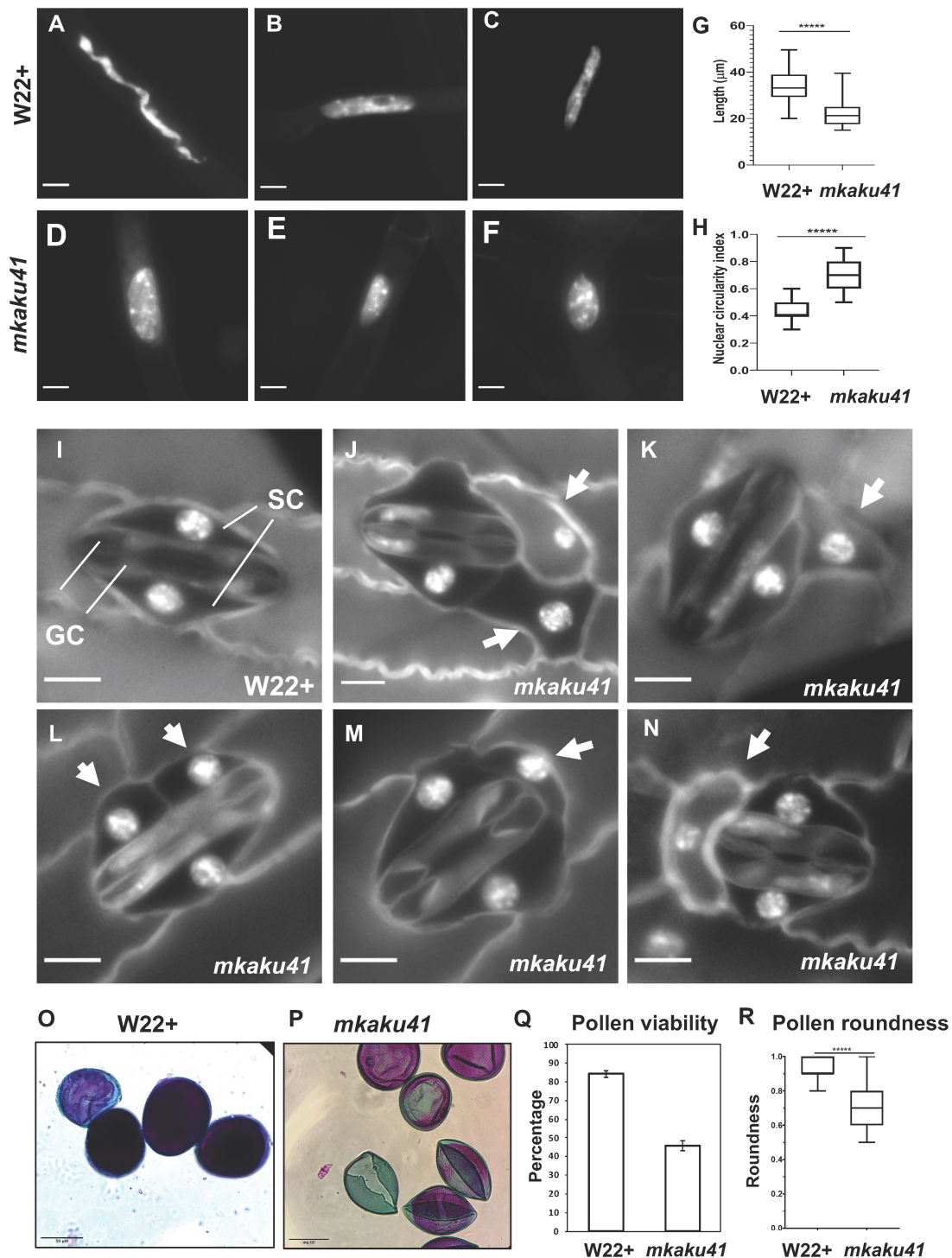


FIGURE 7 | Somatic phenotypes of *mkaku41*. DAPI-stained root hair nuclei in W22+ (**A–C**) and *mkaku41* (**D–F**) seedlings. (**G**) Longest diameter of W22+ and *mkaku41* root hair nuclei ($n = 50$). (**H**) Nuclear circularity index measurements using $4\pi(\text{area}/\text{perimeter}^2)$, where 1 = perfect circle, of W22+ and *mkaku41* root hair nuclei calculated using Fiji. (**I**) Mature stomatal complex in W22+ DAPI-stained leaf where two central dumbbell-shaped guard cells (GC) are surrounded by two subsidiary cells (SC). (**J–N**) Representative images of stomatal complexes in *mkaku41* DAPI-stained leaves. Arrows point to extra or irregularly placed subsidiary cells. Scale bars are 10 μm . ****Student's *t*-test two-tailed, $p < 0.0001$. (**O–Q**) Differential staining of anthers for testing pollen viability from W22+ (**O**) and *mkaku41* -/- (**P,Q**) tassels stained with modified Alexander's stain where viable pollen grains appear magenta and aborted pollen grains appear green. (**R**) Quantification of pollen viability, $n > 1000$ per genotype. (**S**) Degree of pollen roundness $4*\text{area}/(\pi*\text{major_axis}^2)$ calculated for W22+ and *mkaku41* -/- anthers using Fiji. Scale bars are 50 μm . ****Student's *t*-test two-tailed, $p < 0.0001$.

ribosome assembly and scanning, the next in-frame start codon is considerably farther downstream, which would result in a loss of the first 125 AA. Additionally, the mutant 5'UTR may lack regulatory mRNA sequences in the first ~70 bases of the full-length transcript. Further genetic and experimental analyses with new alleles, gene editing, or application of specific biotic or abiotic stresses will be needed to gain a better understanding of how these plant nucleoskeletal proteins functionally interact with the genomes they help to organize.

The regulation of nuclear morphology and intra-nuclear organization was further explored to gain mechanistic insight, using the tobacco transient expression assay with fluorescently tagged proteins and quantitative microscopic analyses. We used this approach to explore multiple aspects of the remarkable nuclear architecture disruption caused by overexpression of each of the three maize nucleoskeletal proteins examined. The severity of the nuclear disruption and of the NE invaginations was increased by co-overexpression of two components (e.g., MKAKU41 with NCH1 or NCH2), or by increasing the transfecting plasmid concentration, expected to increase their expression levels. These findings (Figure 2) and previous studies from plants and animals reveal that proper nucleoskeleton protein concentration may be a primary determinant for overall nuclear architecture (Goto et al., 2014; Legartová et al., 2014; Jorgens et al., 2017).

In addition to protein abundance, components of the nuclear invaginations were tested for the presence of LINC and ER proteins. Knowing that SUN proteins interact with ONM KASH proteins as part of the core LINC complex, we tested whether the intranuclear foci of MKAKU41-FP reflected protein aggregates of entire NE, checking for colocalization with two types of markers, those in the NE but not the LINC complex or those in the ER membrane. All of these, including multiple ONM markers, colocalized with the aberrant intranuclear structures (Figures 4, 5), demonstrating that these intranuclear structures contain components from both the INM and ONM of the nuclear envelope. These plant nuclei invaginations may contain, therefore, the entire NE proteome as well as NE-associated chromatin that would normally be limited to the nuclear periphery. Such invaginations are known to occur in plants and animals, which can show grooves, deformations, actin, or ER in stable structures seen as deep invaginations (Collings et al., 2000; Schermelleh et al., 2008). Interestingly, the membrane invaginations and deformations caused by MKAKU41 also resemble to some extent animal nuclear deformations associated with Lamin-A mis-expression (Lammerding et al., 2004; Schreiber and Kennedy, 2013; Swift et al., 2013; Legartová et al., 2014).

In our experimental set up, we disrupted the LINC complex at two different connections to investigate the effect of these disruptions on the NE structure. The first, a SUN2 Δ N, severed the LINC-to-nucleoskeleton connection; the second MLKS2 Δ ARM, severed the LINC-to-cytoskeleton connection. It is quite interesting that these two disruptions exhibited contrasting effects on the severity of invaginations. Our domain-deletion analyses showed that perturbation of the LINC-to-nucleoskeleton connection *reduced* the severity (Figure 4A),

whereas preventing the LINC-to-cytoskeleton connection *increased* the severity of invaginations (Figure 5). This has important mechanobiological implications for the idea that plant nuclear shape involves a balance of forces between actin-nucleus interactions and nucleoskeletal components. Interestingly, AtKAKU4, arabidopsis KASH proteins WIPs, and NE-associated myosin are all involved in nuclear migration in various cellular processes, such as in pollen-tube growth (Meier et al., 2017; Goto et al., 2020), which also involves changes in actin dynamics.

Moving the nucleus exerts physical stress on the NE and the opposing forces of the LINC components (nucleoskeletal and cytoskeletal) are expected to be, therefore, important for maintaining NE integrity and stability (Enyedi and Niethammer, 2017). The contrasting effects on NE integrity that we observe in this study are an indicator that maize nucleoskeletal components may be functionally associated with just such a tug-of-war process that manifests as regulation of nuclear shape. Multiple lines of evidence are consistent with this idea, including the change to spherical nuclei caused by genetic knockouts of a nuclear-envelope-localized myosin (Tamura et al., 2013) and the rounding up of root hair nuclei caused by the maize *mlks2* mutation (Gumber et al., 2019b). Along these lines, our study adds to the growing body of evidence that plants deploy a general mechanism for nuclear shape in which a balance of forces is achieved through LINC-interacting components on both sides of the NE, ensuring its structure and function as a flexible cellular partition. In the current study, we note multiple indications (Figure 5) that support this tug-of-war type arrangement. These ideas align with results from mammalian studies that identify roles for the LINC complex in mediating mechanical crosstalk between the cytoplasm and nucleus (Alam et al., 2016; Jorgens et al., 2017; Agrawal and Lele, 2019; Bouzid et al., 2019; Hieda, 2019).

Previous investigations of CRWN and KAKU4 have focused on chromatin structure and nuclear architecture (Dittmer et al., 2007; Grob et al., 2014; Hu et al., 2019), but our studies indicate that nucleoplasmic disruptions can also affect normal developmental processes, an important finding for crop species. In animals, the interplay between cellular-level structural integrity and genomic responses to environmental and developmental processes is increasingly recognized as a complex process involving lamins as central players (Gerbino et al., 2018). This study advances our knowledge of the plant nucleoskeleton by identifying the components and their roles in regulating fundamental dynamic processes of the plant nuclear envelope.

MATERIALS AND METHODS

Cloning

Maize gene constructs and sequence information for the clones used in this study are listed in **Supplementary Table 3**. NCH1 ORF was custom-synthesized with *Bam*HI and *Sbf*I at the 5' and 3' ends, respectively (Genscript Biotech Corporation, NJ). The *Bam*HI-NCH1-*Sbf*I construct was sub-cloned by restriction cloning into an ECGFP donor vector containing eGFP-FLAG-HA (Gumber et al., 2019a, JCB), to create the eGFP-FLAG-HA-NCH1 entry vector, named NCH1ec. Similarly,

the *Bam*HI-NCH2-*Pst*I construct was custom synthesized and sub-cloned into an eGFP donor vector to create the eGFP-FLAG-HA-NCH2 entry vector, named NCH2ec. For construction of the mKAKU41 vector, *Bam*HI-mCherry-FLAG-HA-MKAKU41-*Bam*HI was synthesized by Genscript and cloned in pUC18 at the *Bam*HI restriction site. From this cloning vector, the mCherry-FLAG-HA-MKAKU41 gene construct was amplified using KAKUattF (5'-GGGGACAAGTTTGTACAAAAAAGCAGGCTTCATGGTTA GCAAGGGAGAAGAGG-3') and KAKUattR (5'-GGGGACCACTTTGTACAAGAAAGCTGGGTCTCACGTAG CCCGTCCCCGT-3') primers and inserted into pDONR221 vector by BP cloning (Invitrogen), to generate the MKAKU41 entry clone, named MKAKU41ec. For the generation of plant expression vectors, the fluorescent fusion protein constructs from these three entry clones were then transferred individually to the destination vector pH7WG2 (Karimi et al., 2002) by Gate LR recombination (Invitrogen).

For production of the p35S:SP-mCherry-GFP-HDEL positive control for apFRET, mCherry was PCR amplified with Q5 polymerase (NEB) using primers JM403 (5'-GGGGACAAGTTTGTACAAAAAAGCAGGCTACAATGAAA GCCTTACACTCGCTCTCTTCTTAGCTCTTCCCTCTATC TCCTGCCAATCCAGCCATGGTGAGCAAGGGCGAGGAG G-3') and JM404 (5'-acctcactgccaccCTTGTACAGCTCGTCC ATGCCG-3'). The primers included both the Gateway cloning attB1 site and secretion signal at the 5' end, and a 15nt overhang for Gibson assembly at the 3' end, which contained a GGSGG amino acid linker between mCherry and GFP upon fusion. GFP was amplified using primers JM367 (5'-GGGGACCACTTTGTACAAGAAAGCTGGGTGcataattcat catGCTTGTACAGCTCGTCCATGCCGAGAG-3') and JM405 (5'-GTACAAGggtggcagtggaggtATGGTGAGCAAGGGCGAGGA GC-3') which contained the GGSGG linker at the 5' end, and the HDEL ER retention motif, an attB2 site, and a stop codon at the 3' end. These two products were fused together using the NEB HIFI Gibson assembly enzyme mix and incubated at 50°C for 1 h. A Gateway BP reaction into pDONR221 and subsequent LR reaction into pB7FWG2 was then performed to produce the final vector. All steps confirmed by colony PCR and sequencing.

Agrobacterium Transformation

Constructs were transformed into *A. tumefaciens* GV3101. Transformation was performed by incubating plasmid DNA and chemically competent agrobacterium on ice for 30 min, followed by 5 min cold shock in liquid nitrogen, then 5 min heat shock at 37°C in a rotating incubator. After heat shock, 200 µL LB media was added and cells incubated at 28°C for 2 h. Cells were then plated in LB plates containing Spectinomycin (50 µg/mL), Gentamycin (10 µg/mL) and Rifampicin (25 µg/mL) and incubated for 2 days at 28°C. Individual colonies were then picked, grown O/N and transformed into *N. benthamiana*.

Plant Growth Conditions

Nicotiana benthamiana plants were grown in 16:8 h light:dark cycle in a greenhouse maintained at 21°C. Infiltrated plants were 5–6 weeks old.

Live Cell Imaging

Fluorescently tagged proteins of interest were transiently transformed into *N. benthamiana* as described previously (Sparkes et al., 2006). Protein expression constructs first reported here are p35S:NCH1-GFP, p35S:NCH2-GFP and p35S:MKAKU41-mCherry. All other markers have been previously published: p35S:GFP-CNX (Irons et al., 2003), p35S:LBR-GFP (Irons et al., 2003), p35S:MLKP1-GFP (Gumber et al., 2019a), p35S:YFP-AtSUN2 (Graumann et al., 2010), p35S:YFP-AtSUN2ΔNterm (Graumann et al., 2010), p35S:MLKS2-GFP and p35S:MLKS2ΔARM-GFP (Gumber et al., 2019b). An agrobacterium culture of OD 0.1 was used in all conditions unless otherwise stated and cells were imaged 3 days after transformation. The GFP/mCherry combinations were imaged using a Zeiss LSM 800 confocal microscope with line switching, 488 nm and 561 nm excitation, and 500–550 nm and 565–620 nm emissions, collected for GFP and mCherry respectively. For GFP/YFP and YFP/mCherry imaging, a Zeiss LSM 880 was used with frame switching. For GFP/YFP imaging, 488 and 514 nm excitation was used with emission collected between 500–550 and 525–560 for GFP and YFP respectively. For YFP/mCherry imaging, 514 and 561 nm excitation was used, and emission collected between 517–560 nm and 561–624 nm respectively. An image size of 512 × 512 pixels with a scan zoom of 4 and a 63 × 1.4NA lens was used for all imaging described above. All combinations were performed with three independent experimental repeats; representative images are shown. For Fluorescence recovery after photobleaching (FRAP) a 100 × 1.4NA lens was used with a 4 µm ROI in the center of the image, encompassing the nucleus. Five scans were taken pre-bleach and then the 488 nm laser bleached the ROI by using 100% transmission for 20 iterations. Recovery Images were then collected for 1 min to monitor recovery. Data was normalized and FRAP curves produced as described previously (Martiniere et al., 2012).

For acceptor photobleaching Förster resonance energy transfer (apFRET) a 100 × 1.4NA lens was used with a 4 µm ROI in the center of the image, encompassing the nucleus. Five scans were performed with both GFP and mCherry emission/excitation, and then the mCherry construct was bleached in the ROI by the 561 nm laser at 100% transmission for 20 iterations. Following this, five post-bleach scans were taken. Data was normalized and apFRET efficiency (%) calculated as previously (Graumann et al., 2010; Graumann, 2014; Pawar et al., 2016). A minimum of 30 nuclei per condition were used for apFRET across three experimental repeats. A one-way ANOVA was performed to determine statistically significant differences between samples. For Latrunculin-B (LatB) treatment for depolymerization of the actin cytoskeleton, samples were incubated with 25 µM LatB for 1 h, as this has previously been shown to depolymerize the actin cytoskeleton sufficiently (McKenna et al., 2019). Graphs were generated with graphpad as described in the figure legends. Statistical tests were performed in Graphpad Prism and are either ANOVA or Students *T*-test depending on the suitability to the dataset and as specified in the figure legends. For all data sets, ns $p \geq 0.05$, * $p \leq 0.05$, ** $p \leq 0.01$, *** $p \leq 0.001$ and **** $p \leq 0.0001$.

Maize Plant Material and Genotyping

The wild-type W22 used in this study is a color-converted W22 line obtained from Hugo Dooner (Waksman Inst., Rutgers, NJ, United States) derived by Brink (1956). The UF-Mu-00395 seed stock was obtained from the Maize Genetics Cooperation Stock Center¹. The plants were grown at the Florida State University Mission Road Research Facility (Tallahassee, FL, United States) during summer 2017 and 2018, and propagated by out-crossing to W22. In the fall of 2018, the progeny seeds were grown in the greenhouse in the King Life Sciences Building (Biological Science Dept, Florida State University, Tallahassee, FL, United States). The segregating plants were self-crossed to obtain mutant plants from among the progeny.

DNA was isolated from 4-week old seedlings as described previously in Gumber et al. (2019b). PCR genotyping was carried out using a combination of gene-specific forward (F, 5'-CCCGTGAAGCCGAAGGCAGA-3') and reverse (R, 5'-CGCCTCACGCTCACGCTCAC-3') primers, or transposon-specific Tir6 primer (5'-AGAGAAGCCAACGCCAWCGCCTCYATTTTCGTC-3') in combination with F or R primer. The PCR products were resolved by agarose gel electrophoresis and cloned in pCRTM4Blunt-TOPO Vector (Invitrogen cat # K2875-20) by TA cloning. The clones were sequenced and the insert sequences were verified using M13F and M13R vector primers at the Molecular Cloning Facility, Department of Biological Sciences, Florida State University. The sequences were aligned with the W22v2 reference genome to validate the transposon insertion site.

Microscopy in Maize

Maize root hair imaging was carried out as described in Gumber et al. (2019b). Briefly, roots were harvested from 5-day old seedlings and fixed for 1 h in Buffer A (Howe et al., 2013) supplemented with 4% paraformaldehyde. Small sections of root tissue containing root hair were stained with 3 µg/mL DAPI for 20 min at room temperature, mounted with VECTASHIELD, and imaged on an EVOS fluorescence microscope (Thermo Fisher Scientific). The images were processed using the Analyze Particle function of ImageJ to measure the longest diameter and circularity of the nuclei.

For stomatal complex imaging, plants were grown in the greenhouse and the 4th leaf was harvested at its first appearance. The harvested leaf was fixed in Buffer A with 4% paraformaldehyde for an hour at room temperature with rotation. The tissue was rinsed thrice with and stored in Buffer A at 4C, until further use. The leaf tissue was placed on a glass slide, chopped into small pieces and stained with 3 µg/mL DAPI for 20 min at room temperature, mounted with VECTASHIELD, and imaged on an EVOS fluorescence microscope (Thermo Fisher Scientific).

Pollen grain staining was carried out as previously described in Gumber et al. (2019b). Briefly, male flowers were harvested before dehiscence and fixed in Carnoy's fixative (6 alcohol:3 chloroform:1 acetic acid) for a minimum of 2 h at room temperature. Anthers were extruded from flowers with the help

of a micro scalpel and forceps on a glass slide. Staining was carried out with modified Alexander's stain containing Malachite green (0.01%), Acid Fuchsin (0.05%) and Orange G (0.005%) as described to differentiate viable (magenta) pollen grains from aborted (green) pollen grains. Bright field images of the pollen grains were collected on Revolve microscope (Echo Labs). At least 300 pollen grains each from 3 plants of every genotype were counted to calculate pollen viability. Pollen roundness was carried out using Fiji.

RNA Isolation and Library Preparation

Segregating wildtype and mutant mkaku41 plants were grown in the greenhouse. From 2 week-old plants, fourth leaves were harvested and from 6 to 8 week old plants, mid-prophase meiotic-staged male flowers were harvested. The tissues were immediately stored in liquid nitrogen. RNA was isolated from three biological replicates for each genotype using Qiagen RNeasy Plant mini kit per manufacturer's instructions. Integrity of the RNA was tested using the Bioanalyzer (Agilent) system. For library preparation, sample input was 400 ng total RNA (determined by Qubit RNA HS reagents, Thermo) with RIN > 7 (Bioanalyzer RNA Nano, Agilent). Libraries were prepared with the Biomek 400 Automated Workstation (Beckman Coulter), using the NEBNext Ultra II RNA Library Prep kit for Illumina (New England Biolabs) according to manufacturer's instructions, with an RNA fragmentation time of 15 min, a 1/10th dilution of NEB adaptor and 11 cycles of PCR amplification with dual-indexing primers. Amplified libraries were initially quantified by Qubit DNA HS reagents, checked for size and artifacts using Bioanalyzer DNA HS reagents, and KAPA qPCR (KAPA Biosystems) was used to determine molar quantities of each library. Individual libraries were diluted and pooled equimolar, and the pool was again checked by Bioanalyzer and KAPA qPCR before submission for sequencing.

RNA Sequencing and Data Analysis

RNA-seq libraries were sequenced on a Novaseq 6000 at the Translational Science Lab, College of Medicine, Florida State University. Approximately 40 million single-end 100 base reads were obtained for each biological replicate in this experiment and are available from NCBI sequence read archive project, accession number PRJNA675860. Contaminating 3' adapter sequences were trimmed from the demultiplexed raw reads using cutadapt version 1.16. Raw and trimmed reads were subjected to quality control testing with fastqc. Trimmed reads were aligned to the W22 genome assembly "Zm-W22-REFERENCE-NRGENE-2.0" using the splice-aware aligner hisat2. Briefly, Hisat2 indices were constructed from known exons, and splice sites extracted from the W22 genome annotation (Zm00004b) and the reference genome assembly (Zm-W22-REFERENCE-NRGENE-2.0.fasta). Trimmed reads were then aligned to the resulting splice-aware hisat2 index using the following optional arguments: `-rna-strandness R`, `-dta-cufflinks`, `-summary-file`. Predicted novel transcripts were assembled and merged across replicates and samples using stringtie2 in "conservative" mode. Per-transcript coverage tables were prepared by stringtie2 in "ballgown" format. Resulting coverage tables were converted into count tables

¹<http://maizecoop.crops.ci.uiuc.edu/>

suitable for differential expression analysis by DESeq2 in R using the tximport package. Differential expression analysis was performed separately for each tissue group, i.e. (leaf mutant vs. WT and tassel mutant vs. WT). Briefly, genes with fewer than 10 counts across all replicates were discarded and DESeq2 results were generated for both tissue groups such that $\log_2(\text{fold-change})$ estimates were reported for (mutant/WT) ratios. Statistically significant differentially expressed (adjusted p -value < 0.05) genes were subsequently extracted from each of the resulting DESeq2 tables for further analysis (**Supplementary Table 2**).

DATA AVAILABILITY STATEMENT

The original sequence data used in this study are publicly available from NCBI accession PRJNA675860.

AUTHOR CONTRIBUTIONS

The expression plasmids made by HG and HB and used by JM and KG for cytological analysis. The tobacco transient expression microscopy data was produced and images collected by JM with image analysis by JM and KG. The maize mutant analysis, PCR genotyping, all cloning, and RNA isolation was done by HG, the maize phenotyping was done by AJ, AK, HG, and HB. The transcriptome analysis and SRA curation were done by ZT and HB. The experiments were designed, interpreted, and written about by JM, HG, ZT, KG, and HB. All the authors have read and approved the manuscript.

FUNDING

This work was performed as part of the Cost action # CA16212 'INDEPTH' whose members are appreciated for their fruitful discussions. This work was supported in part by a grant to HB from the National Science Foundation (NSF IOS 1444532).

ACKNOWLEDGMENTS

We would like to acknowledge the Bioimaging unit at Oxford Brookes for access to the confocal microscopes.

REFERENCES

- Agrawal, A., and Lele, T. P. (2019). Mechanics of nuclear membranes. *J. Cell Sci.* 132:jcs229245. doi: 10.1242/jcs.229245
- Alam, S. G., Zhang, Q., Prasad, N., Li, Y., Chamala, S., Kuchibhotla, L., et al. (2016). The mammalian LINC complex regulates genome transcriptional responses to substrate rigidity. *Sci. Rep.* 6: 38063.
- Bouazid, T., Kim, E., Riehl, B. D., Esfahani, A. M., Rosenbohm, J., Yang, R., et al. (2019). The LINC complex, mechanotransduction, and mesenchymal stem cell function and fate. *J. Biol. Eng.* 13:68.
- Brink, R. A. (1956). A genetic change associated with the R locus in maize which is directed and potentially reversible. *Genetics* 41, 872–889. doi: 10.1093/genetics/41.6.872
- Chang, W., Worman, H. J., and Gundersen, G. G. (2015). Accessorizing and anchoring the LINC complex for multifunctionality. *J. Cell Biol.* 208, 11–22. doi: 10.1083/jcb.201409047
- Choi, J., Strickler, S. R., and Richards, E. J. (2019). Loss of CRWN nuclear proteins induces cell death and salicylic acid defense signaling. *Plant Physiol.* 179, 1315–1329. doi: 10.1104/pp.18.01020
- Ciska, M., and Moreno Di-az de la Espina, S. (2014). The intriguing plant nuclear lamina. *Front. Plant Sci.* 5:166.

SUPPLEMENTARY MATERIAL

The Supplementary Material for this article can be found online at: <https://www.frontiersin.org/articles/10.3389/fpls.2021.645218/full#supplementary-material>

Supplementary Figure 1 | The Maize NCH1 and NCH2 proteins co-localize with their Arabidopsis homolog CRWN1. **(A)** Confocal live cell imaging of cells co-expressing either NCH1 or NCH2 with Arabidopsis CRWN1 shows colocalization. **(B)** Plot of raw FRAP intensity values over time for two representative FRAP experiments: one for NCH1 (black) and one for NCH2 (red). **(C)** Normalized intensity data plotted for all NCH1 FRAP curves. Blue points show individual data points, black lines show FRAP curve fits for each nucleus, and red lines show global FRAP curves produced from all datasets (As shown in **Figure 1**). **(D)** Same as panel C except for NCH2. **(E)** Box plots of FRAP recovery plateau values for NCH1 and NCH2. **(F)** Box plots of FRAP recovery half-time values for NCH1 and NCH2. For panels **E** and **F**, the individual data points from single FRAP recovery curves (black dots), the mean (red line), standard deviations (blue lines), and statistical significance (asterisks) are indicated. Students T -test performed in **E** and **F**, ** $p \leq 0.01$, *** $p \leq 0.0001$. Mean and standard deviation values are tabulated below the plots. $n \geq 30$ nuclei imaged across three experimental repeats.

Supplementary Figure 2 | Description of Sub-periphery/whole nuclei fluorescence ratio measurement. Diagram describing how the sub-periphery over whole nuclei measurement was determined using image J. Two regions of interest (ROIs) were generated, one encompassing the whole nuclei and one only sub-periphery nuclear fluorescence (yellow ROIs with hashed boundaries). The sub-periphery fluorescence value was then divided by the whole nuclei fluorescence value in order to obtain the ratio. If the majority of fluorescence is located at the periphery/nuclear envelope, this would result in a low ratio, conversely if most fluorescence was internal, this would result in a higher ratio.

Supplementary Figure 3 | Multiple Seq Alignment of Transcripts. **(A)** The 5' UTR region and a small portion of the CDS are diagrammed as shown in **Figure 5**, and reversed (bottom configuration) as aligned in the multiple sequence alignment. **(B)** The multiple sequence alignment displays all of the RNA-seq reads with a perfect match to the 25 bp query sequence (yellow) using grep of the fastq files. All matches were converted to FASTA sequences for multiple sequence alignment. The reference genome sequence is shown at top for comparison. The sequence identifiers start with single characters for tissue ("L" for leaf; "T" for tassel), genotype ("1" for wildtype, "2" for mkaku41 homozygous mutant), or bioreplicate ("A," "B," or "C" for bioreplicate 1, 2, or 3, respectively), followed by unique identifier from Illumina sequence read name. The strandedness is indicated relative to the gene model, with all antisense RNAs indicated (ANTISENSE, red text).

Supplementary Table 1 | Values for apFRET efficiency with Internal controls and multiple comparisons of all treatments. **(A)** All apFRET efficiency% values for data presented in **Figure 3C** including internal control values. **(B)** Tukey multiple comparison one way Anova dataset from all apFRET data presented, including that presented in **Figure 3C**.

Supplementary Table 2 | Differentially expressed genes between *mkaku41* mutant versus wildtype plants for maize leaf and tassel.

Supplementary Table 3 | Plasmid information and Addgene IDs.

- Ciska, M., Hikida, R., Masuda, K., and Moreno Díaz de la Espina, S. (2019). Evolutionary history and structure of nuclear matrix constituent proteins, the plant analogues of lamins. *J. Exp. Bot.* 70, 2651–2664. doi: 10.1093/jxb/erz102
- Collings, D. A., Carter, C. N., Rink, J. C., Scott, A. C., Wyatt, S. E., Allen, N. S., et al. (2000). Plant nuclei can contain extensive grooves and invaginations. *Plant Cell* 12, 2425–2440. doi: 10.2307/3871239
- Crisp, M., Liu, Q., Roux, K., Rattner, J. B., Shanahan, C., Burke, B., et al. (2006). Coupling of the nucleus and cytoplasm: role of the LINC complex. *J. Cell Biol.* 172, 41–53. doi: 10.1083/jcb.200509124
- De Magistris, P., and Antonin, W. (2018). The dynamic nature of the nuclear envelope. *Curr. Biol.* 28, R487–R497.
- Dittmer, T. A., Stacey, N. J., Sugimoto-Shirasu, K., and Richards, E. J. (2007). Little nuclei genes affecting nuclear morphology in *Arabidopsis thaliana*. *Plant Cell* 19, 2793–2803. doi: 10.1105/tpc.107.053231
- Enyedi, B., and Niethammer, P. (2017). Nuclear membrane stretch and its role in mechanotransduction. *Nucleus* 8, 156–161. doi: 10.1080/19491034.2016.1263411
- Evans, D. E., and Graumann, K. (2018). *The Linker of Nucleoskeleton and Cytoskeleton Complex In Higher Plants*. Hoboken, NJ: John Wiley.
- Gerbino, A., Procino, G., Svelto, M., and Carosino, M. (2018). Role of lamin A/C gene mutations in the signaling defects leading to cardiomyopathies. *Front. Physiol.* 9:1356.
- Goto, C., Tamura, K., Fukao, Y., Shimada, T., and Hara-Nishimura, I. (2014). The novel nuclear envelope protein KAKU4 modulates nuclear morphology in *Arabidopsis*. *Plant Cell* 26, 2143–2155. doi: 10.1105/tpc.113.122168
- Goto, C., Tamura, K., Nishimaki, S., Maruyama, D., and Hara-Nishimura, I. (2020). The nuclear envelope protein KAKU4 determines the migration order of the vegetative nucleus and sperm cells in pollen tubes. *J. Exp. Bot.* 71, 6273–6281. doi: 10.1093/jxb/eraa367
- Graumann, K. (2014). Evidence for LINC1-SUN Associations at the plant nuclear periphery. *PLoS One* 9:e93406. doi: 10.1371/journal.pone.0093406
- Graumann, K., and Evans, D. E. (2017). “The nuclear envelope - structure and protein interactions,” in *Annual Plant Reviews Online*, ed. J. A. Roberts, (Chichester: John Wiley & Sons, Ltd), 19–56. doi: 10.1002/9781118472507.ch2
- Graumann, K., Runions, J., and Evans, D. E. (2010). Characterization of SUN-domain proteins at the higher plant nuclear envelope. *Plant J.* 61, 134–144. doi: 10.1111/j.1365-313x.2009.04038.x
- Grob, S., Schmid, M. W., and Grossniklaus, U. (2014). Hi-C analysis in *Arabidopsis* identifies the KNOT, a structure with similarities to the flamenco locus of *Drosophila*. *Mol. Cell* 55, 678–693. doi: 10.1016/j.molcel.2014.07.009
- Gumber, H. K., McKenna, J. F., Estrada, A. L., Jalovec, A. M., Kartick, A. C., and Graumann, K. (2019a). Identification and characterization of genes encoding the nuclear envelope LINC complex in the monocot species *Zea mays*. *J. Cell Sci.* 132:jcs221390. doi: 10.1242/jcs.221390
- Gumber, H. K., McKenna, J. F., Tolmie, A. F., Jalovec, A. M., Kartick, A. C., and Graumann, K. (2019b). MLKS2 is an ARM domain and F-actin-associated KASH protein that functions in stomatal complex development and meiotic chromosome segregation. *Nucleus* 10, 144–166. doi: 10.1080/19491034.2019.1629795
- Guo, T., Mao, X., Zhang, H., Zhang, Y., Fu, M., and Sun, Z. (2017). Lamin-like proteins negatively regulate plant immunity through NAC with transmembrane motif1-like9 and nonexpressor of PR genes1 in *Arabidopsis thaliana*. *Mol. Plant* 10, 1334–1348. doi: 10.1016/j.molp.2017.09.008
- Hagan, I., and Yanagida, M. (1995). The product of the spindle formation gene *sad1* associates with the fission yeast spindle pole body and is essential for viability. *J. Cell Biol.* 129, 1033–1047. doi: 10.1083/jcb.129.4.1033
- Haque, F., Lloyd, D. J., Smallwood, D. T., Dent, C. L., Shanahan, C. M., and Fry, A. M. (2006). SUN1 interacts with nuclear lamin A and cytoplasmic nesprins to provide a physical connection between the nuclear lamina and the cytoskeleton. *Mol. Cell Biol.* 26, 3738–3751. doi: 10.1128/mcb.26.10.3738-3751.2006
- Hetzler, M. W. (2010). The nuclear envelope. *Cold Spring Harb. Perspect. Biol.* 2, a000539–a000539.
- Hieda, M. (2019). Signal Transduction across the nuclear envelope: role of the LINC complex in bidirectional signaling. *Cells* 8:124. doi: 10.3390/cells8020124
- Howe, E. S., Murphy, S. P., and Bass, H. W. (2013). “Three-dimensional acrylamide fluorescence in situ hybridization for plant cells” in *Plant Meiosis: Methods and Protocols*, eds W. P. Pawlowski, M. Grelon, and S. Armstrong, (Totowa, NJ: Humana Press), 53–66. doi: 10.1007/978-1-62703-333-6_6
- Hu, B., Wang, N., Bi, X., Karaaslan, E. S., Weber, A. L., and Zhu, W. (2019). Plant lamin-like proteins mediate chromatin tethering at the nuclear periphery. *Genome Biol.* 20:87.
- Irons, S. L., Evans, D. E., and Brandizzi, F. (2003). The first 238 amino acids of the human lamin B receptor are targeted to the nuclear envelope in plants. *J. Exp. Bot.* 54, 943–950. doi: 10.1093/jxb/erg102
- Janin, A., Bauer, D., Ratti, F., Millat, G., and Mejat, A. (2017). Nuclear envelopopathies: a complex LINC between nuclear envelope and pathology. *Orphanet J. Rare Dis.* 12:147.
- Jorgens, D. M., Inman, J. L., Wojcik, M., Robertson, C., Palsdottir, H., and Tsai, W. T. (2017). Deep nuclear invaginations are linked to cytoskeletal filaments – integrated bioimaging of epithelial cells in 3D culture. *J. Cell Sci.* 130, 177–189. doi: 10.1242/jcs.190967
- Karimi, M., Inzé, D., and Depicker, A. (2002). Gateway vectors for agrobacterium-mediated plant transformation. *Trends Plant Sci.* 7, 193–195. doi: 10.1016/s1360-1385(02)02251-3
- Kim, D. I., Ke, B., and Roux, K. J. (2015). Making the linc: sun and kash protein interactions. *Biol. Chem.* 396, 295–310. doi: 10.1515/hsz-2014-0267
- Lammerding, J., Schulze, P. C., Takahashi, T., Kozlov, S., Sullivan, T., and Kamm, R. D. (2004). Lamin A/C deficiency causes defective nuclear mechanics and mechanotransduction. *J. Clin. Invest.* 113, 370–378. doi: 10.1172/jci200419670
- Legartová, S., Stixová, L., Laur, O., Kozubek, S., Sehnalova, P., and Bartova, E. (2014). Nuclear structures surrounding internal lamin invaginations: morphology of internal lamins. *J. Cell. Biochem.* 115, 476–487. doi: 10.1002/jcb.24681
- Leppek, K., Das, R., and Barna, M. (2018). Functional 5' UTR mRNA structures in eukaryotic translation regulation and how to find them. *Nat. Rev. Mol. Cell Biol.* 19, 158–174. doi: 10.1038/nrm.2017.103
- Luxton, G. G., and Starr, D. A. (2014). KASHing up with the nucleus: novel functional roles of KASH proteins at the cytoplasmic surface of the nucleus. *Curr. Opin. Cell Biol.* 28, 69–75. doi: 10.1016/j.ceb.2014.03.002
- Malone, C. J., Fixsen, W. D., Horvitz, H. R., and Han, M. (1999). UNC-84 localizes to the nuclear envelope and is required for nuclear migration and anchoring during *C. elegans* development. *Dev. Camb. Engl.* 126, 3171–3181.
- Martiniere, A., Lavagi, I., Nageswaran, G., Rolfe, D. J., Maneta-Peyret, L., and Luu, D. T. (2012). Cell wall constrains lateral diffusion of plant plasma-membrane proteins. *Proc. Natl. Acad. Sci. U.S.A.* 109, 12805–12810. doi: 10.1073/pnas.1202040109
- Masuda, K., Xu, Z. J., Takahashi, S., Ono, M., Nomura, K., and Inoue, M. (1997). Peripheral framework of carrot cell nucleus contains a novel protein predicted to exhibit a long alpha-helical domain. *Exp. Cell Res.* 232, 173–181. doi: 10.1006/excr.1997.3531
- McCarty, D. R., and Meeley, R. B. (2009). “Transposon resources for forward and reverse genetics in maize,” in *Handbook of Maize*, eds J. L. Bennetzen, and S. Hake, (New York, NY: Springer), 561–584. doi: 10.1007/978-0-387-77863-1_28
- McKenna, J. F., Rolfe, D. J., Webb, S. E. D., Tolmie, A. F., Botchway, S. W., and Martin-Fernandez, M. L. (2019). The cell wall regulates dynamics and size of plasma-membrane nanodomains in *Arabidopsis*. *Proc. Natl. Acad. Sci. U.S.A.* 116, 12857–12862. doi: 10.1073/pnas.1819077116
- Meier, I., Richards, E. J., and Evans, D. E. (2017). Cell biology of the plant nucleus. *Annu. Rev. Plant Biol.* 68, 139–172. doi: 10.1146/annurev-arplant-042916-041115
- Murphy, S. P., Simmons, C. R., and Bass, H. W. (2010). Structure and expression of the maize (*Zea mays* L.). SUN-domain protein gene family: evidence for the existence of two divergent classes of SUN proteins in plants. *BMC Plant Biol.* 10:269. doi: 10.1186/1471-2229-10-269
- Newman-Griffis, A. H., del Cerro, P., Charpentier, M., and Meier, I. (2019). Medicago LINC complexes function in nuclear morphology, nuclear movement, and root nodule symbiosis. *Plant Physiol.* 179, 491–506. doi: 10.1104/pp.18.01111
- Pawar, V., Poulet, A., Détourné, G., Tatout, C., Vanrobays, E., and Evans, D. E. (2016). A novel family of plant nuclear envelope-associated proteins. *J. Exp. Bot.* 67, 5699–5710.
- Pradillo, M., Evans, D., and Graumann, K. (2019). The nuclear envelope in higher plant mitosis and meiosis. *Nucleus* 10, 55–66. doi: 10.1080/19491034.2019.1587277

- Rothballer, A., and Kutay, U. (2013). The diverse functional LINC's of the nuclear envelope to the cytoskeleton and chromatin. *Chromosoma* 122, 415–429. doi: 10.1007/s00412-013-0417-x
- Sakamoto, Y. (2020). Nuclear lamina CRWN proteins regulate chromatin organization, gene expression, and nuclear body formation in plants. *J. Plant Res.* 133, 457–462. doi: 10.1007/s10265-020-01184-1
- Schermelleh, L., Carlton, P. M., Haase, S., Shao, L., Winoto, L., and Kner, P. (2008). Subdiffraction multicolor imaging of the nuclear periphery with 3D structured illumination microscopy. *Science* 320, 1332–1336. doi: 10.1126/science.1156947
- Schreiber, K. H., and Kennedy, B. K. (2013). When lamins go bad: nuclear structure and disease. *Cell* 152, 1365–1375. doi: 10.1016/j.cell.2013.02.015
- Sparkes, I. A., Runions, J., Kearns, A., and Hawes, C. (2006). Rapid, transient expression of fluorescent fusion proteins in tobacco plants and generation of stably transformed plants. *Nat. Protoc.* 1, 2019–2025. doi: 10.1038/nprot.2006.286
- Starr, D. A. (2002). Role of ANC-1 in tethering nuclei to the actin cytoskeleton. *Science* 298, 406–409. doi: 10.1126/science.1075119
- Starr, D. A. (2019). A network of nuclear envelope proteins and cytoskeletal force generators mediates movements of and within nuclei throughout *Caenorhabditis elegans* development. *Exp. Biol. Med.* 244, 1323–1332. doi: 10.1177/1535370219871965
- Starr, D. A., and Fridolfsson, H. N. (2010). Interactions between nuclei and the cytoskeleton are mediated by SUN-KASH nuclear-envelope bridges. *Annu. Rev. Cell Dev. Biol.* 26, 421–444. doi: 10.1146/annurev-cellbio-100109-104037
- Swift, J., Ivanovska, I. L., Buxboim, A., Harada, T., Dingal, P. C., and Pinter, J. (2013). Nuclear lamin-a scales with tissue stiffness and enhances matrix-directed differentiation. *Science* 341, 1240104–1240104. doi: 10.1126/science.1240104
- Tamura, K., Goto, C., and Hara-Nishimura, I. (2015). Recent advances in understanding plant nuclear envelope proteins involved in nuclear morphology. *J. Exp. Bot.* 66, 1641–1647. doi: 10.1093/jxb/erv036
- Tamura, K., Iwabuchi, K., Fukao, Y., Kondo, M., Okamoto, K., and Ueda, H. (2013). Myosin XI-i links the nuclear membrane to the cytoskeleton to control nuclear movement and shape in *Arabidopsis*. *Curr. Biol.* 23, 1776–1781. doi: 10.1016/j.cub.2013.07.035
- Wang, H., Dittmer, T. A., and Richards, E. J. (2013). *Arabidopsis* crowded nuclei (crwn) proteins are required for nuclear size control and heterochromatin organization. *BMC Plant Biol.* 13:200. doi: 10.1186/1471-2229-13-200
- Zhang, X., Zhao, M., McCarty, D. R., and Lisch, D. (2020). Transposable elements employ distinct integration strategies with respect to transcriptional landscapes in eukaryotic genomes. *Nucleic Acids Res.* 48, 6685–6698. doi: 10.1093/nar/gkaa370
- Zhao, W., Guan, C., Feng, J., Liang, Y., Zhan, N., and Zuo, J. (2016). The *Arabidopsis* crowded nuclei genes regulate seed germination by modulating degradation of ABI5 protein: CRWNs regulate seed germination. *J. Integr. Plant Biol.* 58, 669–678. doi: 10.1111/jipb.12448
- Zhou, X., Graumann, K., Wirthmueller, L., Jones, J. D., and Meier, I. (2014). Identification of unique SUN-interacting nuclear envelope proteins with diverse functions in plants. *J. Cell Biol.* 205, 677–692. doi: 10.1083/jcb.201401138

Conflict of Interest: The authors declare that the research was conducted in the absence of any commercial or financial relationships that could be construed as a potential conflict of interest.

Copyright © 2021 McKenna, Gumber, Turpin, Jalovec, Kartick, Graumann and Bass. This is an open-access article distributed under the terms of the Creative Commons Attribution License (CC BY). The use, distribution or reproduction in other forums is permitted, provided the original author(s) and the copyright owner(s) are credited and that the original publication in this journal is cited, in accordance with accepted academic practice. No use, distribution or reproduction is permitted which does not comply with these terms.

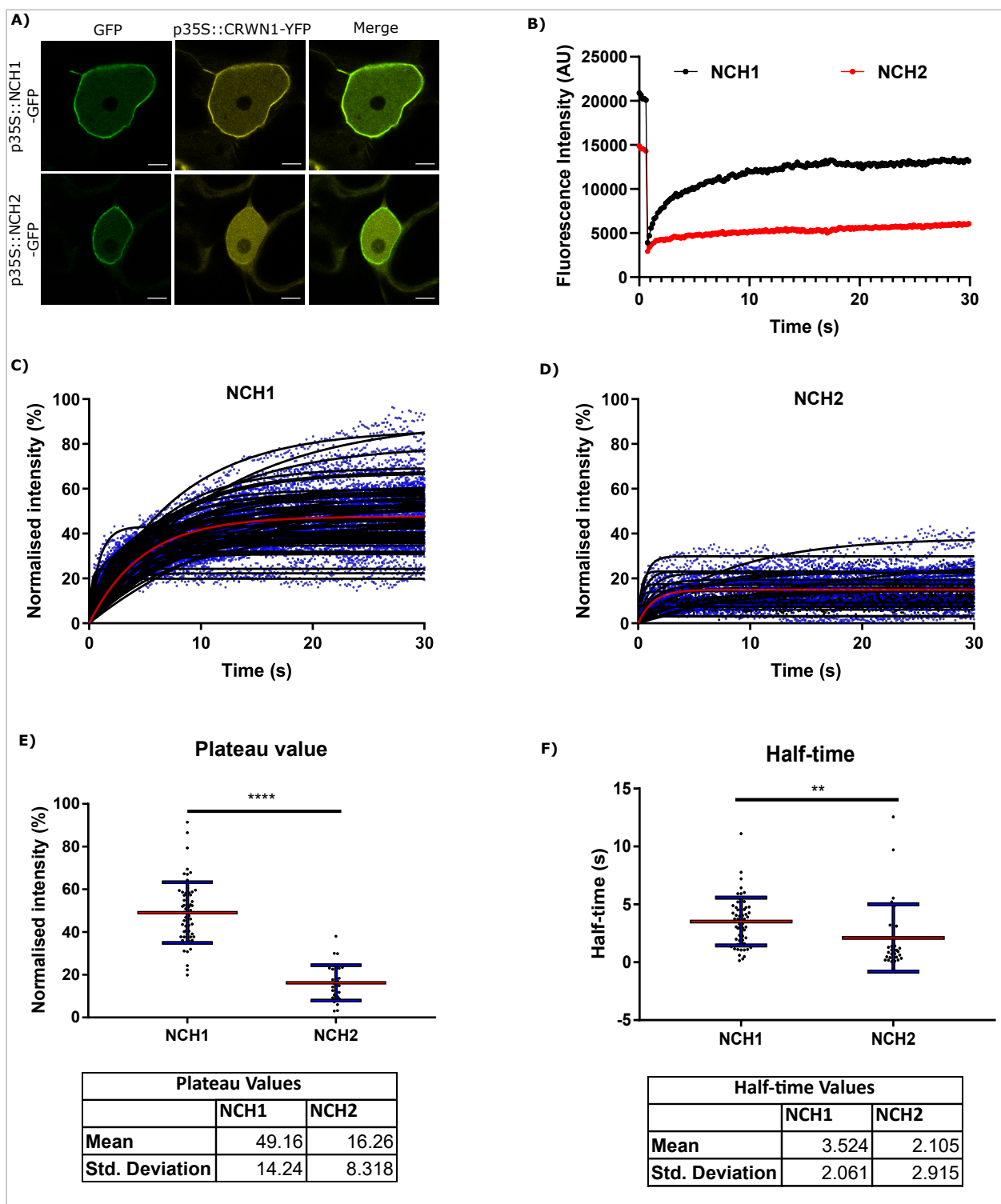


Figure S1
(McKenna, Gumber, et al., *FIPS*, 2021)

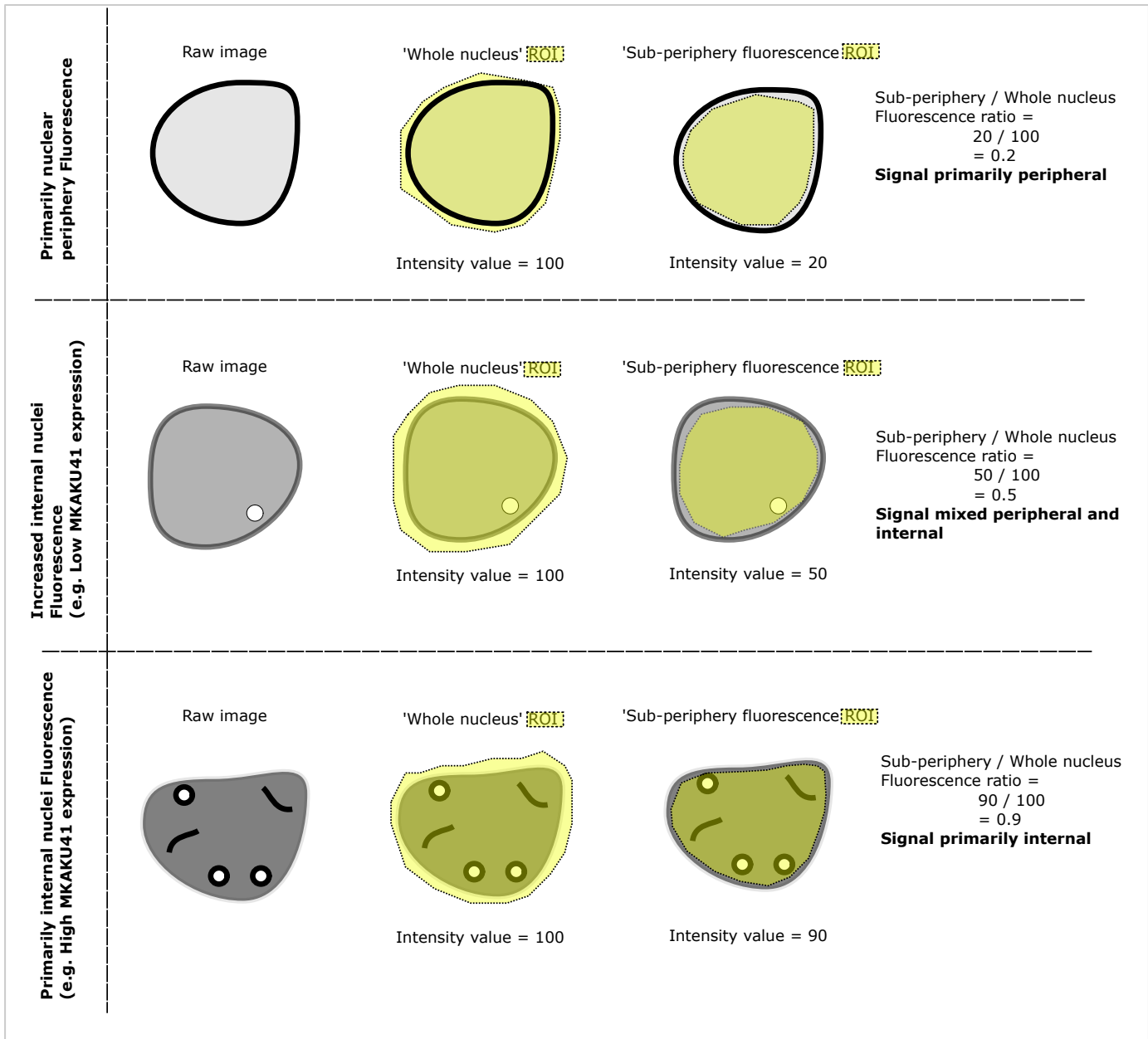


Figure S2
(McKenna, Gumber, et al., *FiPS*, 2021)

Supp Table S1: Values for apFRET efficiency with Internal controls and multiple comparisons of all treatments.

A)	NCH1 & CNX	NCH1 & CNX IC	NCH1 & KAKU41	NCH1 & KAKU41 IC	NCH2 & CNX	NCH2 & CNX IC	NCH2 & KAKU41	NCH2 & KAKU41 IC	CNX & KAKU41	CNX & KAKU41 IC	mCherry -GFP -HDEL	mCherry -GFP -HDEL IC
Number of values	30	30	30	30	30	30	33	33	30	30	30	30
Mean FRET Efficiency (%)	1.4	-0.67	10	-0.94	3.3	-0.86	11	-0.76	6.6	-2.1	19	-0.9
Std. Deviation	3.7	0.53	2.4	0.3	2.7	0.4	3	0.35	4.6	0.63	6.8	1.3
Std. Error of Mean	0.67	0.097	0.43	0.055	0.5	0.074	0.53	0.061	0.84	0.11	1.2	0.23

B)	Mean Diff.	95.00% CI of diff.	Below threshold?	Summary	Adjusted P Value
Tukey's multiple comparisons test					
NCH1 & CNX vs. NCH1 & CNX IC	2.073	-0.4343 to 4.580	No	ns	0.2208
NCH1 & CNX vs. NCH1 & KAKU41	-8.939	-11.45 to -6.432	Yes	****	<0.0001
NCH1 & CNX vs. NCH1 & KAKU41 IC	2.343	-0.1640 to 4.850	No	ns	0.0925
NCH1 & CNX vs. NCH2 & CNX	-1.874	-4.381 to 0.6311	No	ns	0.3694
NCH1 & CNX vs. NCH2 & CNX IC	2.263	-0.2439 to 4.770	No	ns	0.122
NCH1 & CNX vs. NCH2 & KAKU41	-9.607	-12.06 to -7.158	Yes	****	<0.0001
NCH1 & CNX vs. NCH2 & KAKU41 IC	2.163	-0.2862 to 4.612	No	ns	0.1434
NCH1 & CNX vs. CNX & KAKU41	-5.199	-7.706 to -2.692	Yes	****	<0.0001
NCH1 & CNX vs. CNX & KAKU41 IC	3.473	0.9662 to 5.980	Yes	***	0.0004
NCH1 & CNX vs. mCherry -GFP -HDEL	-17.14	-19.65 to -14.64	Yes	****	<0.0001
NCH1 & CNX vs. mCherry -GFP -HDEL IC	2.303	-0.2041 to 4.810	No	ns	0.1065
NCH1 & CNX IC vs. NCH1 & KAKU41	-11.01	-13.52 to -8.505	Yes	****	<0.0001
NCH1 & CNX IC vs. NCH1 & KAKU41 IC	0.2703	-2.237 to 2.777	No	ns	>0.9999
NCH1 & CNX IC vs. NCH2 & CNX	-3.946	-6.453 to -1.440	Yes	****	<0.0001
NCH1 & CNX IC vs. NCH2 & CNX IC	0.1905	-2.316 to 2.697	No	ns	>0.9999
NCH1 & CNX IC vs. NCH2 & KAKU41	-11.68	-14.13 to -9.230	Yes	****	<0.0001
NCH1 & CNX IC vs. NCH2 & KAKU41 IC	0.09053	-2.359 to 2.540	No	ns	>0.9999
NCH1 & CNX IC vs. CNX & KAKU41	-7.272	-9.779 to -4.765	Yes	****	<0.0001
NCH1 & CNX IC vs. CNX & KAKU41 IC	1.401	-1.106 to 3.907	No	ns	0.7958
NCH1 & CNX IC vs. mCherry -GFP -HDEL	-19.22	-21.72 to -16.71	Yes	****	<0.0001
NCH1 & CNX IC vs. mCherry -GFP -HDEL IC	0.2303	-2.277 to 2.737	No	ns	>0.9999
NCH1 & KAKU41 vs. NCH1 & KAKU41 IC	11.28	8.775 to 13.79	Yes	****	<0.0001
NCH1 & KAKU41 vs. NCH2 & CNX	7.065	4.558 to 9.572	Yes	****	<0.0001
NCH1 & KAKU41 vs. NCH2 & CNX IC	11.2	8.695 to 13.71	Yes	****	<0.0001
NCH1 & KAKU41 vs. NCH2 & KAKU41	-0.6675	-3.117 to 1.782	No	ns	0.9991
NCH1 & KAKU41 vs. NCH2 & KAKU41 IC	11.1	8.653 to 13.55	Yes	****	<0.0001
NCH1 & KAKU41 vs. CNX & KAKU41	3.74	1.233 to 6.247	Yes	****	<0.0001
NCH1 & KAKU41 vs. CNX & KAKU41 IC	12.41	9.905 to 14.92	Yes	****	<0.0001
NCH1 & KAKU41 vs. mCherry -GFP -HDEL	-8.204	-10.71 to -5.698	Yes	****	<0.0001
NCH1 & KAKU41 vs. mCherry -GFP -HDEL IC	11.24	8.735 to 13.75	Yes	****	<0.0001
NCH1 & KAKU41 IC vs. NCH2 & CNX	-4.217	-6.724 to -1.710	Yes	****	<0.0001
NCH1 & KAKU41 IC vs. NCH2 & CNX IC	-0.07984	-2.587 to 2.427	No	ns	>0.9999
NCH1 & KAKU41 IC vs. NCH2 & KAKU41	-11.95	-14.40 to -9.500	Yes	****	<0.0001
NCH1 & KAKU41 IC vs. NCH2 & KAKU41 IC	-0.1798	-2.629 to 2.270	No	ns	>0.9999
NCH1 & KAKU41 IC vs. CNX & KAKU41	-7.542	-10.05 to -5.035	Yes	****	<0.0001
NCH1 & KAKU41 IC vs. CNX & KAKU41 IC	1.13	-1.377 to 3.637	No	ns	0.9444
NCH1 & KAKU41 IC vs. mCherry -GFP -HDEL	-19.49	-21.99 to -16.98	Yes	****	<0.0001
NCH1 & KAKU41 IC vs. mCherry -GFP -HDEL IC	-0.04004	-2.547 to 2.467	No	ns	>0.9999
NCH2 & CNX vs. NCH2 & CNX IC	4.137	1.630 to 6.644	Yes	****	<0.0001
NCH2 & CNX vs. NCH2 & KAKU41	-7.733	-10.18 to -5.284	Yes	****	<0.0001
NCH2 & CNX vs. NCH2 & KAKU41 IC	4.037	1.588 to 6.486	Yes	****	<0.0001
NCH2 & CNX vs. CNX & KAKU41	-3.325	-5.832 to -0.8183	Yes	**	0.001
NCH2 & CNX vs. CNX & KAKU41 IC	5.347	2.840 to 7.854	Yes	****	<0.0001
NCH2 & CNX vs. mCherry -GFP -HDEL	-15.27	-17.78 to -12.76	Yes	****	<0.0001
NCH2 & CNX vs. mCherry -GFP -HDEL IC	4.177	1.670 to 6.684	Yes	****	<0.0001
NCH2 & CNX IC vs. NCH2 & KAKU41	-11.87	-14.32 to -9.421	Yes	****	<0.0001
NCH2 & CNX IC vs. NCH2 & KAKU41 IC	-0.09992	-2.549 to 2.349	No	ns	>0.9999
NCH2 & CNX IC vs. CNX & KAKU41	-7.462	-9.969 to -4.955	Yes	****	<0.0001
NCH2 & CNX IC vs. CNX & KAKU41 IC	1.21	-1.297 to 3.717	No	ns	0.9125
NCH2 & CNX IC vs. mCherry -GFP -HDEL	-19.41	-21.91 to -16.90	Yes	****	<0.0001
NCH2 & CNX IC vs. mCherry -GFP -HDEL IC	0.0398	-2.467 to 2.547	No	ns	>0.9999
NCH2 & KAKU41 vs. NCH2 & KAKU41 IC	11.77	9.380 to 14.16	Yes	****	<0.0001
NCH2 & KAKU41 vs. CNX & KAKU41	4.408	1.958 to 6.857	Yes	****	<0.0001
NCH2 & KAKU41 vs. CNX & KAKU41 IC	13.08	10.63 to 15.53	Yes	****	<0.0001
NCH2 & KAKU41 vs. mCherry -GFP -HDEL	-7.537	-9.986 to -5.088	Yes	****	<0.0001
NCH2 & KAKU41 vs. mCherry -GFP -HDEL IC	11.91	9.460 to 14.36	Yes	****	<0.0001
NCH2 & KAKU41 IC vs. CNX & KAKU41	-7.362	-9.812 to -4.913	Yes	****	<0.0001
NCH2 & KAKU41 IC vs. CNX & KAKU41 IC	1.31	-1.139 to 3.759	No	ns	0.8385
NCH2 & KAKU41 IC vs. mCherry -GFP -HDEL	-19.31	-21.76 to -16.86	Yes	****	<0.0001
NCH2 & KAKU41 IC vs. mCherry -GFP -HDEL IC	0.1397	-2.310 to 2.589	No	ns	>0.9999
CNX & KAKU41 vs. CNX & KAKU41 IC	8.672	6.165 to 11.18	Yes	****	<0.0001
CNX & KAKU41 vs. mCherry -GFP -HDEL	-11.94	-14.45 to -9.438	Yes	****	<0.0001
CNX & KAKU41 vs. mCherry -GFP -HDEL IC	7.502	4.995 to 10.01	Yes	****	<0.0001
CNX & KAKU41 IC vs. mCherry -GFP -HDEL	-20.62	-23.12 to -18.11	Yes	****	<0.0001
CNX & KAKU41 IC vs. mCherry -GFP -HDEL IC	-1.17	-3.677 to 1.337	No	ns	0.9296
mCherry -GFP -HDEL vs. mCherry -GFP -HDEL IC	19.45	16.94 to 21.95	Yes	****	<0.0001

* Note IC = Internal FRET efficiency control

Table S2: Differentially expressed genes between *mkaku41* mutant versus wildtype plants for maize leaf and tassel.

Table S2 (Tab 1 of 2) LEAF DEGs. All **225** Differentially Expressed Genes from Leaf.

W22v2 GeneID	B73v3 GeneID	B73v4 GeneID	Phytomine description	Uniprot id	Uniprot descriptor	baseMean-LEAF	log2FoldChange (mutant/WT)	lfcSE	stat	pvalue	padj
Zm00004b022952	GRMZM2G079381	Zm00001d052165	(1 of 2) K00366 - fe#N/A	#N/A	#N/A	7467.22638	29.4246738	3.90677062	7.53171267	5.01E-14	4.72E-11
Zm00004b029478	GRMZM2G442804	Zm00001d036738	(1 of 2) 2.1.1.163 - lB4FF4A	S-adenosyl-L-methi	S-adenosyl-L-methi	828.430667	13.1270875	3.61827211	3.62799898	0.000286	0.02374659
Zm00004b031378	GRMZM2G163861	Zm00001d039141	(1 of 4) PTHR2405:AOA1D6MDU6	Mitogen-activated p	Mitogen-activated p	801.772225	13.0798895	3.63809059	3.59526219	0.000324	0.02627982
Zm00004b032719	GRMZM2G039586	Zm00001d046354	(1 of 2) PTHR1007:B4F991	GATA transcription f	GATA transcription f	675.803091	12.8333192	3.58881725	3.57591882	0.000349	0.02800135
Zm00004b002158	GRMZM2G050961	Zm00001d029997	(1 of 3) PTHR1077:B4FBN1	Chloroplast chaper	Chloroplast chaper	666.3195	12.8129119	3.61916377	3.54029624	4.00E-04	3.14E-02
Zm00004b031472	GRMZM2G154664	Zm00001d044745	(1 of 1) PTHR11777:AOA1D6NR62	Alanine--tRNA ligas	Alanine--tRNA ligas	442.856807	12.2235394	3.60460055	3.39109402	6.96E-04	4.88E-02
Zm00004b038561	GRMZM2G052036	Zm00001d024241	AOA1D6IYD1	Uncharacterized pr	Uncharacterized pr	412.427315	12.1208047	1.25435573	9.6629723	4.33E-22	1.07E-18
Zm00004b024341	GRMZM2G119932	Zm00001d0533848	(1 of 5) PF00646/PK7U803	Protein SRG1	Protein SRG1	221.633368	11.2250547	1.22916079	9.13229154	6.71E-20	1.21E-16
Zm00004b040326	GRMZM2G148495	Zm00001d026354	K7TSM1	Uncharacterized pr	Uncharacterized pr	155.731123	10.7159853	2.56855691	4.17198672	0.000302	0.00390509
Zm00004b030713	GRMZM2G150471	Zm00001d038361	(1 of 2) PTHR1282:AOA1D6MSQ9	Protein Y1PF	Protein Y1PF	144.117489	10.6047446	1.29299803	8.20167116	2.37E-16	3.35E-13
Zm00004b038977	GRMZM2G000361	Zm00001d021708	(1 of 146) PF13812:AOA1D6IE64	Pentatricopeptide r	Pentatricopeptide r	91.6284647	9.95055033	2.55206086	3.89092548	0.000966	0.01021058
Zm00004b002460	GRMZM2G018929	Zm00001d030398	(1 of 2) PTHR2401:AOA1D6KCE5	Pentatricopeptide r	Pentatricopeptide r	73.3024849	9.62871858	2.01775461	4.77199682	0.0000182	0.000344
Zm00004b037691	GRMZM2G020401	Zm00001d022604	(1 of 1) KOG3444 - C4J9F3	SNARE-like superfi	SNARE-like superfi	65.4345211	9.46628094	1.2787588	7.92271029	1.33E-13	9.78E-11
Zm00004b028573	GRMZM2G133629	Zm00001d035319	AOA1D6LFF8	Uncharacterized pr	Uncharacterized pr	61.0798391	9.3646218	1.24462084	7.52407602	5.31E-14	4.78E-11
Zm00004b012339	GRMZM2G048904	Zm00001d014596	(1 of 3) 2.3.1.98 - C:AOA1D6GUF2	Alpha-L-fucosidase	Alpha-L-fucosidase	49.0004256	9.04879444	1.54416675	5.85998553	4.63E-09	0.00001447
Zm00004b012010	GRMZM2G042136	Zm00001d014157	(1 of 6) K03809 - N.B6SPB2	Flavoprotein wrbA	Flavoprotein wrbA	45.2989985	8.93336195	1.23319652	7.24407002	4.35E-13	2.87E-10
Zm00004b029741	GRMZM2G142443	Zm00001d037085	C4J5G0	Uncharacterized pr	Uncharacterized pr	43.6925677	8.88172812	1.25055644	7.10222093	1.23E-12	7.36E-10
Zm00004b030995	GRMZM2G044368	Zm00001d038709	(1 of 5) K07897 - R:AOA1D6M9Y7	Ras-related protein	Ras-related protein	854.281322	8.80825777	2.49236587	3.534095	0.000409	0.03185181
Zm00004b006605	GRMZM2G129261	Zm00001d002654	(1 of 3) PTHR1059:AOA1D6E325	Naked endosperm1	Naked endosperm1	793.787161	8.69986561	0.80718841	10.7779863	4.37E-27	2.16E-23
Zm00004b015807	GRMZM2G380319	Zm00001d039492	AOA1D6MHP7	Myb-like transcripti	Myb-like transcripti	892.089428	8.9050629	1.78182041	4.65282935	3.27E-06	0.000573
Zm00004b015016	GRMZM2G090419	Zm00001d017951	(1 of 4) 3.6.1.13/3:lB4FG54	Nudix hydrolase 17	Nudix hydrolase 17	26.4253106	8.15810576	1.40186465	5.8194675	5.90E-09	1.74E-06
Zm00004b031301	GRMZM2G141252	Zm00001d039054	(1 of 5) PTHR1009:#N/A	#N/A	#N/A	90.5160879	8.08452683	1.15322615	7.01035681	2.38E-12	1.38E-09
Zm00004b000717	GRMZM2G471253	Zm00001d028138	(1 of 3) PF04481 - lAOA1D6JSB5	Thiamine monopho	Thiamine monopho	70.5305127	7.71803729	1.08519142	7.11214369	1.14E-12	7.06E-10
Zm00004b036815	GRMZM2G069928	Zm00001d021532	(1 of 1) K01931 - pr:AOA1D6BIW0	RING/U-box superfi	RING/U-box superfi	67.482069	7.66883779	1.29122334	5.992032	2.86E-09	9.89E-07
Zm00004b013399	GRMZM2G177404		(1 of 4) 1.1.1.35/4:#N/A	#N/A	#N/A	16.2942554	7.46088293	1.8357165	4.064293	0.000482	0.00584858
Zm00004b002499	GRMZM2G878022	Zm00001d030507	AOA1D6KCL1	WAT1-related prote	WAT1-related prote	16.1201044	7.44434477	1.29028755	5.76952384	7.95E-09	0.000023
Zm00004b004054	GRMZM2G413853	Zm00001d032655	(1 of 1) PTHR1495:AOA1D6KSK7	Dicer-like 102	Dicer-like 102	8.91036307	6.59202137	1.39215016	4.73513676	0.0000219	0.000409
Zm00004b034409	GRMZM2G420926	Zm00001d048336	(1 of 2) PTHR1166:AOA1D6PJC8	Serine/threonine-pr	Serine/threonine-pr	766.748915	6.50183669	1.65029566	6.39980112	0.000815	0.00886601
Zm00004b037350	GRMZM2G312954	Zm00001d022184	(1 of 4) K17964 - le:AOA1D6IK37	Putative pentatricop	Putative pentatricop	7.96421792	6.43041896	1.58590284	4.02932986	0.000559	0.00654916
Zm00004b036573	GRMZM2G052474	Zm00001d021248	(1 of 2) PTHR1394:B7ZZ58	NC domain-contain	NC domain-contain	7.83785058	6.40412598	1.6734301	3.82694562	0.00013	0.01277228
Zm00004b0025146	GRMZM2G112686	Zm00001d008829	(1 of 1) PTHR2283:AOA1D6FGP9	GDG esterase/lipa	GDG esterase/lipa	6.32065121	6.10773003	1.64375468	3.70990701	0.00207	0.01831493
Zm00004b004163	GRMZM2G379656	Zm00001d032784	(1 of 1) PTHR2640:AOA1D6KTY7	Two-component res	Two-component res	6.27782711	6.08247491	1.39072809	4.37359033	0.0000122	0.00175244
Zm00004b038551	GRMZM2G017013	Zm00001d021221	(1 of 6) PTHR1232:BDT.JD1	Protein binding2	Protein binding2	72.3278301	6.27320731	1.72986443	3.47939926	0.000513	0.03814297
Zm00004b018053	GRMZM2G432390	Zm00001d042397	(1 of 15) 3.6.3.43 - lAOA1D6N311	ABC transporter B f	ABC transporter B f	612.986352	5.99792177	1.29237744	4.64099851	0.0000347	0.000586
Zm00004b000836	GRMZM2G344416	Zm00001d028274	(1 of 3) PTHR1017:AOA1D6JU49	Cyclin-SDS	Cyclin-SDS	5.65464364	5.93097241	1.51373161	3.9181136	0.000892	0.00954532
Zm00004b024850	GRMZM2G112968	Zm00001d008529	(1 of 7) 3.1.30.1 - A:AOA1D6FDT0	Endonuclease 2	Endonuclease 2	178.036732	5.89782245	1.22968922	4.79618944	0.0000162	0.000308
Zm00004b006533	GRMZM2G038851	Zm00001d002570	(1 of 7) K10577 - ut:AOA1D6E1Y4	SUMO-conjugating	SUMO-conjugating	5.44743536	5.87866260	1.61415843	3.64193511	2.71E-04	2.29E-02
Zm00004b039730	GRMZM2G038834	Zm00001d025670	(1 of 2) PTHR2334:AOA1D6J8H8	Glycerophosphodie	Glycerophosphodie	5.34966121	5.85600702	1.47791992	3.96233039	7.42E-05	8.23E-03
Zm00004b027306	GRMZM2G091973	Zm00001d011631	(1 of 2) PTHR1099:B7ZY13	Reticulon-like prote	Reticulon-like prote	5.3177009	5.83749437	1.59890571	3.65093095	0.000261	0.02228524
Zm00004b007542	GRMZM2G589609	Zm00001d003783	#N/A	#N/A	#N/A	4.99512044	5.75176401	1.53940107	3.73636484	1.87E-04	1.69E-02
Zm00004b009893	GRMZM2G096106	Zm00001d006845	(1 of 2) K14288 - e:AOA1D6F180	Exportin-T (Export	Exportin-T (Export	4.74289835	5.67384186	1.57729911	3.59718828	3.22E-04	0.0261934
Zm00004b021274	GRMZM2G085573	Zm00001d050051	(1 of 3) PTHR2305:AOA1D6PZJ6	Calcineurin subunit	Calcineurin subunit	4.65262088	5.64877774	1.44916835	3.89794445	0.000097	0.01021058
Zm00004b016770	GRMZM2G895400		(1 of 2) PF07516 - #N/A	#N/A	#N/A	4.63320769	5.52897694	1.52920236	3.61595935	0.0003	0.04260305
Zm00004b024230	GRMZM2G000976	Zm00001d053719	(1 of 2) PTHR1106:AOA1D6QRU0	Exostosin-like	Exostosin-like	3.6831895	5.30796093	1.53300346	3.46363272	0.000533	0.03920133
Zm00004b037809	GRMZM2G036918	Zm00001d023301	(1 of 20) K13648 - i:AOA1D6IRJ1	Hexosyltransferase	Hexosyltransferase	12.9621521	5.24927925	1.29524929	4.05271732	0.000506	0.00599844
Zm00004b020964	GRMZM2G036829	Zm00001d049343	(1 of 2) PTHR1334:AOA1D6PTV7	Glutamy-l-RNA red.	Glutamy-l-RNA red.	428.130074	5.2109914	0.56562159	9.21285867	3.18E-20	6.28E-17
Zm00004b017828	GRMZM2G170689	Zm00001d042150	(1 of 4) 3.1.2.12 - S:AOA1D6N1Q6	S-formylglutathione	S-formylglutathione	28.670786	5.05967754	0.88129422	5.74119001	9.40E-09	0.00002686
Zm00004b000729	GRMZM2G047513	Zm00001d028153	(1 of 1) PTHR1170:AOA1D6JSF1	30S ribosomal prote	30S ribosomal prote	214.616897	4.43378056	1.1150952	3.97614531	0.00007	0.00796499
Zm00004b013031	GRMZM2G058252	Zm00001d015460	(1 of 2) K11098 - sn:AOA1D6H288	Putative small nucle	Putative small nucle	89.9045646	4.40178796	1.16074364	3.79221374	0.000149	0.01420386
Zm00004b018106	GRMZM2G013016	Zm00001d042472	(1 of 9) PF03514 - AOA1D6N495	Protein SCARECRK	Protein SCARECRK	7.5468871	4.38419021	1.26130462	3.47591704	0.000509	0.03801417
Zm00004b021544	GRMZM2G068455	Zm00001d050409	(1 of 2) PTHR1154:BF4V33	MAP kinase	MAP kinase	154.545715	4.27985353	1.17886939	3.63047303	0.000283	0.02361936
Zm00004b010999	GRMZM2G585405	Zm00001d013012	(1 of 2) PTHR2156:AOA1D6GEW1	HIT zinc finger	HIT zinc finger	46.8177556	3.90744209	1.03999381	3.75717822	0.000172	0.01574167
Zm00004b036912	GRMZM2G180082	Zm00001d021639	(1 of 1) 1.14.13.184:AOA1D6ID92	Taxane 13-alpha-hy	Taxane 13-alpha-hy	32.4905967	3.89379865	0.64241747	6.08116561	1.35E-09	4.95E-07
Zm00004b016491	GRMZM2G121404	Zm00001d040311	(1 of 5) K12619 - 5:AOA1D6MQ12	5'-3' exonbinucleot	5'-3' exonbinucleot	17.6527176	3.5797071	0.52159871	3.88426215	0.000103	0.01062917
Zm00004b027586	GRMZM2G460566	Zm00001d011938	K7VM12	Uncharacterized pr	Uncharacterized pr	174.944398	3.48226135	0.30138449	11.55427157	7.03E-31	6.95E-27
Zm00004b005210	GRMZM2G348578	Zm00001d034124	(1 of 1) PTHR1086:AOA1D6L5N8	Putative prolyl 4-hy	Putative prolyl 4-hy	13.4450367	3.42875627	0.8513486	4.02744102	5.64E-05	6.56E-03
Zm00004b040037	GRMZM2G322634	Zm00001d026025	AOA1D6JBS5	Uncharacterized pr	Uncharacterized pr	40.7950382	3.38071759	0.81575384	4.14428647	3.41E-05	4.32E-03
Zm00004b024374	GRMZM2G155370	Zm00001d0533880	(1 of 52) PF06203 - AOA1D6QT42	Protein CHLOROPI	Protein CHLOROPI	61.9716189	3.36826757	0.88969286	3.78587684	0.000153	0.01443203
Zm00004b038737	GRMZM2G133512	Zm00001d024470	(1 of 1) PTHR2085:AOA1D6IZI0	DNA-directed RNA	DNA-directed RNA	60.9752615	3.18589191	0.43383499	7.34355683	2.08E-13	1.42E-10
Zm00004b013023	GRMZM2G109818	Zm00001d015450	(1 of 2) K19347 - SI:AOA1D6H268	SUN domain protei	SUN domain protei	163.827706	3.0935191	0.8914755	3.47011118	0.00052	0.03841063
Zm00004b032080	GRMZM2G350319	Zm00001d045492	(

Zm00004b039163	GRMZM2G330635	Zm00001d024963	(1 of 2) PTHR1126 B6TL20	Glutathione S-trans	821.559951	1.12368212	0.25566698	4.39510063	0.0000111	0.00162285
Zm00004b040552	GRMZM2G343149	Zm00001d028606	(1 of 2) KOG0716 - C4J426	DNAJ heat shock N	175.191177	1.11399665	0.19553823	5.69707843	1.22E-08	0.00000335
Zm00004b006763	GRMZM2G394450	Zm00001d002830	(1 of 3) PF11837 - IAOA1D6E4N9	Beta-fructofuranosyl	510.860825	1.04284275	0.25253867	4.68611918	0.00000278	0.000492
Zm00004b032888	GRMZM2G069630	Zm00001d046571	(1 of 4) PTHR2304 AOA1D6P3H5	Putative HLH DNA-	435.078325	1.01298064	0.15126213	6.69685548	2.13E-11	1.11E-08
Zm00004b028605	GRMZM2G410757	Zm00001d035456	AOA1D6LGG0	Uncharacterized pr	1102.34203	0.94624438	0.24964589	3.79034631	0.00015	0.01424261
Zm00004b023489	GRMZM2G002220	Zm00001d052809	(1 of 4) K09487 - hK7V364	Heat shock protein	1163.42188	0.94580231	0.15748147	6.00580049	1.90E-09	6.73E-07
Zm00004b030504	GRMZM2G305851	Zm00001d038085	(1 of 10) PF11891 - AOA1D6M325	Protein RETICULA	1188.38199	0.9352027	0.22602528	4.13760226	0.0000351	0.00442314
Zm00004b005417	GRMZM2G074404	Zm00001d034432	(1 of 2) PTHR2329 B6TIC8	Bax inhibitor-1 fami	424.535285	0.86562979	0.19919175	4.34571109	1.39E-05	1.93E-03
Zm00004b028575	GRMZM2G143788	Zm00001d035321	(1 of 4) PTHR1384 B6T2N1	SWIB/MDM2 doma	489.708705	0.85679437	0.23070118	3.71387084	0.000204	0.01811114
Zm00004b018769	GRMZM2G173654	Zm00001d043234	(1 of 1) PTHR1261 AOA1D6N9M7	NTF2-like	282.736689	0.82559477	0.24273462	0.24212386	0.000671	0.04740744
Zm00004b016582	GRMZM2G111014	Zm00001d040416	(1 of 1) K02470 - DIAOA1D6MQM1	DNA topoisomerase	573.22022	0.79663319	0.14929919	5.33581713	9.51E-08	2.35E-05
Zm00004b003782	GRMZM2G127396	Zm00001d032334	(1 of 1) PTHR2409 AOA1D6KQ39	Phospholipid-transf	307.752055	0.79617809	0.17445876	4.56370378	5.03E-06	8.29E-04
Zm00004b027549	GRMZM2G046558	Zm00001d011891	(1 of 1) K01070 - S-K7V5R6	S-formylglutathione	527.285315	0.76070436	0.19834295	3.8352982	0.000125	0.01244172
Zm00004b021214	GRMZM2G090241	Zm00001d049956	(1 of 2) K00215 - 4-AOA1D6PYZ9	4-hydroxy-tetrahyd	112.382554	0.73587653	0.19995354	3.68023762	0.000233	0.02013407
Zm00004b040222	GRMZM2G129071	Zm00001d026244	(1 of 2) PTHR3022 B7ZY2	Putrescine-binding	282.623632	0.72752977	0.21154612	3.43910705	0.000584	0.04230188
Zm00004b026760	GRMZM2G086766	Zm00001d010969	(1 of 2) KOG3882 - COPGJ5	Tetraspanin-6	207.76703	0.69786407	0.18917115	3.68906184	2.25E-04	1.97E-02
Zm00004b025751	GRMZM2G158818	Zm00001d009719	(1 of 2) PTHR1383 AOA1D6FLA0	PPM-type phosphat	532.830662	0.63346597	0.17343334	3.65250396	0.00026	0.02224501
Zm00004b038221	GRMZM2G036427	Zm00001d023830	(1 of 1) PTHR3196 B6TLW3	Protein Fb19	1662.27079	-0.4159396	0.11035950	-3.7689666	1.64E-04	1.52E-02
Zm00004b011092	GRMZM2G007260	Zm00001d013092	(1 of 5) K10573 - utB4FH08	Ubiquitin-conjugatir	923.813124	-0.4178773	0.12114084	-3.4495159	0.000562	0.04100456
Zm00004b012273	AC207656_3_FG00	Zm00001d014507	(1 of 17) PF02362 AOA1D6GTV0	Auxin response fac	516.855693	-0.4187385	0.12013197	-3.485654	0.000491	0.0369359
Zm00004b038722	AC207722_2_FG00	Zm00001d021435	(1 of 7) K08912 - IqB4FNR1	Chlorophyll a-b bin	1709.12.219	-0.4331024	0.11385239	-3.8040698	0.000142	0.01373875
Zm00004b023254	GRMZM2G119175	Zm00001d052494	(1 of 2) PTHR1181 AOA1D6QHK1	Pyruvate kinase (E	839.32923	-0.475611	0.12467717	-3.8147405	0.000136	0.01322287
Zm00004b012904	GRMZM2G425774	Zm00001d015293	(1 of 2) PTHR2173 AOA1D6H134	VIN3-like protein 2	197.522432	-0.6919321	0.19597291	-3.5307537	0.000414	0.03202049
Zm00004b019820	GRMZM2G339540	Zm00001d044434	(1 of 16) PF00069 AOA1D6NLS2	Putative inactive re	227.937947	-0.7314427	0.14663392	-4.9882229	0.000000609	0.000131
Zm00004b038201	GRMZM2G001500	Zm00001d023802	(1 of 3) PTHR1937 AOA1D6IW15	Heat shock 70 kDa	390.383872	-0.7427689	0.16663045	-4.4575823	8.29E-06	1.28E-03
Zm00004b040507	GRMZM2G124466	Zm00001d026543	(1 of 14) PF04755 - AOA1D6JH82	Putative plastid-lip	580.51809	-0.8379358	0.16072008	-5.2136345	0.000000185	0.0000436
Zm00004b024839	GRMZM2G033034	Zm00001d008817	(1 of 8) PTHR1985 AOA1D6FDQ9	Actin-interacting pr	325.234613	-0.8419972	0.14369917	-5.8594439	6.44E-09	0.00000414
Zm00004b029016	GRMZM2G110983	Zm00001d036054	(1 of 5) K10573 - utAOA1D6LKH9	Ubiquitin-conjugatir	428.180372	-0.9107724	0.14663329	-5.112252	5.26E-10	2.21E-07
Zm00004b031450	GRMZM2G310569	Zm00001d044717	(1 of 2) PTHR1021 K7VQ87	Potassium outward	776.082506	-0.9308469	0.17592059	-5.2912904	1.21E-07	2.90E-05
Zm00004b039612	GRMZM2G132875	Zm00001d025533	(1 of 3) PTHR1173 K7TP18	NAD(P)-linked oxid	470.476633	-0.9542234	0.25513441	-3.7400811	0.000184	0.01677345
Zm00004b019130	GRMZM2G158013	Zm00001d043614	(1 of 1) PTHR1181 AOA1D6NDM6	Putative sulfate tra	220.659598	-0.9996597	0.28788078	-3.4724782	5.16E-04	3.82E-02
Zm00004b0201942	GRMZM2G165231	Zm00001d050947	(1 of 1) PTHR2325 C0P3M4	Protein kinase supe	268.98269	-1.1283469	0.30233028	-3.7322261	1.90E-04	1.71E-02
Zm00004b023416	GRMZM2G097043	Zm00001d052723	(1 of 1663) 2.7.11.1 AOA1D6QJ79	Uncharacterized pr	483.959303	-1.1750113	0.3058207	-3.8421574	0.000122	0.01218775
Zm00004b031824	GRMZM2G301860	Zm00001d045204	(1 of 2) PTHR3172 K7W642	Putative AP2/EREB	91.8123203	-1.1767874	0.26793309	-4.3920943	1.12E-05	1.63E-03
Zm00004b020891	GRMZM2G145972	Zm00001d049897	(1 of 6) K17871 - N.AOA1D6PWC3	External alternative	425.719275	-1.2024434	0.34440027	-3.4914125	0.00048	0.03636419
Zm00004b014169	GRMZM2G132706	Zm00001d016942	(1 of 1) PTHR1192 AOA1D6HBD6	Glycosyltransferase	86.7275892	-1.2785948	0.33703593	-3.7936455	1.48E-04	0.01419039
Zm00004b012181	GRMZM2G035405	Zm00001d014377	(1 of 19) PF02309 AOA1D6GSR8	Auxin response fac	150.839573	-1.3074657	0.2772201	-4.7163544	0.0000024	0.00044
Zm00004b028942	GRMZM2G145396	Zm00001d035948	(1 of 1) PF06592 - IAOA1D6LJT8	ATOZ1I	154.479925	-1.3600375	0.30840566	-4.409898	0.0000103	0.00155207
Zm00004b025175	GRMZM2G464891	Zm00001d008963	(1 of 2) PTHR1260 AOA1D6FGW1	GD11 family protei	130.802281	-1.3936656	0.2822666	-4.9374087	0.000000792	0.001163
Zm00004b040292	GRMZM2G145460	Zm00001d026311	(1 of 3) K12448 - UIAOA1D6JE16	NAD(P)-binding Ro	64.5436053	-1.3980243	0.32470084	-4.3055765	0.0000167	0.00225723
Zm00004b000015	GRMZM2G105436	Zm00001d027416	(1 of 1) 1.3.99.22 - IAOA1D6JM25	Oxygen-independe	71.9333728	-1.4589138	0.32542419	-4.4831158	0.00000736	0.00117383
Zm00004b024901	GRMZM2G477503	Zm00001d008600	(1 of 39) PF00534 - AOA1D6FE41	Sulfoquinovosyl tra	135.498723	-1.4788108	0.38764344	-3.8148739	0.000136	0.01322297
Zm00004b001193	GRMZM2G443265	Zm00001d028713	(1 of 2) PTHR11132 B4F896	Putative sugar phos	146.819959	-1.7099847	0.36230074	-4.7197936	0.00000236	0.000437
Zm00004b031260	GRMZM2G318180	Zm00001d039011	(1 of 2) PTHR1016 AOA1D6MVC5	Grx_11-glutaredoxir	55.4236579	-1.728671	0.43620094	-3.9629385	0.0000074	0.00823089
Zm00004b021606	GRMZM2G370915	Zm00001d050484	(1 of 4) PTHR1076 AOA1D6Q1U4	Transmembrane 9 ;	24.9518867	-1.7731962	0.51670068	-3.4317667	0.0006	0.04330487
Zm00004b031166	GRMZM2G010349	Zm00001d038894	(1 of 1) PTHR1158 AOA1D6MBR1	Serine/threonine-pr	7526.21654	-1.8467058	0.44452862	-4.1543013	0.0000236	0.00416527
Zm00004b030125	GRMZM2G009845	Zm00001d037606	(1 of 4) PF00514 P/COP5C0	Importin subunit alp	672.163686	-1.8509677	0.41775015	-4.430801	0.00000939	0.00144006
Zm00004b031291	GRMZM2G065757	Zm00001d039043	(1 of 4) PTHR1368 AOA1D6MD15	Aspartic proteinase	895.396897	-1.8789325	0.39154149	-4.7988801	0.0000016	0.000307
Zm00004b034200	GRMZM2G132395	Zm00001d048112	(1 of 4) PTHR1313 CAJAV5	RING/U-box superf	14.9266987	-1.9881288	0.58232065	-3.4141479	0.00064	0.04570428
Zm00004b031703	GRMZM2G177098	Zm00001d045054	(1 of 2) 4.2.3.123 - IAOA1D6NT87	Sesquiterpene cycl	563.977223	-2.023258	0.44239875	-4.7090051	0.00000249	0.000452
Zm00004b023346	GRMZM2G091258	Zm00001d052620	(1 of 3) PF15346 - IAOA1D6FUY0	Uncharacterized pr	84.8148844	-2.0969343	0.51434005	-4.0769415	0.0000256	0.0050862
Zm00004b009147	GRMZM2G066615	Zm00001d005917	(1 of 18) PF04784 - AOA1D6ERJ3	Ternary complex fa	52.1992731	-2.1476846	0.60276371	-3.5630622	3.67E-04	2.91E-02
Zm00004b038557	GRMZM2G134613	Zm00001d024239	(1 of 4) K08341 - G.AOA1D6IYD0	Autophagy-related J	220.308776	-2.1764262	0.29327857	-7.42102	1.16E-13	8.84E-11
Zm00004b010118	GRMZM2G473709	Zm00001d007174	AOA1D6F4F7	Uncharacterized pr	72.7028661	-2.2070216	0.60999614	-3.6180911	2.97E-04	2.45E-02
Zm00004b016247	GRMZM2G360023	Zm00001d039993	(1 of 5) 1.11.1.6 - C B6SUS4	Uncharacterized pr	54.6089476	-2.4961955	0.66210963	-3.7700637	0.000163	0.01522807
Zm00004b014100	GRMZM2G113453	Zm00001d016856	(1 of 15) PF07887 - AOA1D6HAV0	Calmodulin binding	896.773245	-2.5156699	0.56352855	-4.4641393	0.0000084	0.00126316
Zm00004b039718	GRMZM2G173878	Zm00001d025660	(1 of 4) K07877 - R#N1A	#N1A	97.9240301	-2.5712222	0.5819074	-4.3428253	0.0000141	0.00194446
Zm00004b009434	GRMZM2G158629	Zm00001d006270	(1 of 2) KOG1206 - C4JA75	Enoyl-CoA hydratase	85.256169	-2.5476031	0.72103652	-3.5332512	0.00041	0.03185181
Zm00004b001295	GRMZM2G076537	Zm00001d028827	(1 of 1) PTHR1305 AOA1D6K021	Enuclease DPD1	11.6682028	-2.589785	0.67760974	-3.8219417	1.32E-04	1.30E-02
Zm00004b011960	GRMZM2G146446	Zm00001d014109	(1 of 1) PTHR1431 AOA1D6GPFY5	Transmembrane pr	47.2813877	-2.634432	0.57927246	-4.5478289	5.42E-06	8.86E-04
Zm00004b000177	GRMZM2G090051	Zm00001d027443	(1 of 9) 1.14.13.129 AOA1D6JM56	Hydroxylase8	165.877537	-2.6361802	0.48594064	-5.4249018	0.00000058	0.0001497
Zm00004b018443	GRMZM2G585658	Zm00001d042841	(1 of 2) K08193 - M B6SWK6	Putative anion trans	69.729378	-2.6900368	0.43660711	-6.1612919	7.22E-10	2.69E-07
Zm00004b039626	GRMZM2G104603	Zm00001d025549	B4FV84	Putative carboxyles	16.7476499	-2.7905884	0.70460708	-3.9604887	0.0000748	0.00823089
Zm00004b038619	GRMZM2G315767	Zm00001d024317	(1 of 2) PTHR3164 AOA1D6IYR6	Transferase	26.921785	-2.006855	0.4854769	-6.1936108	5.88E-10	2.33E-07
Zm00004b000094	GRMZM2G077769	Zm00001d027346	(1 of 61) PF02298 - AOA1D6LJL9	Early nodulin-like pr	16.7445831	-3.0378518	0.61567127	-4.9342107	8.05E	

Zm00004b018231	GRMZM2G025703	Zm00001d042613	(1 of 2) PTHR1061:A0A1D6N5E7	RING/FYVE/PHD- η	5.558418	-5.931268	1.52727424	-3.8835645	0.000103	0.01062619
Zm00004b015220	GRMZM2G021514	Zm00001d018189	(1 of 1) PF00400/P.A0A1D6HLB9	Major facilitator sup	5.65292164	-5.9470806	1.54429679	-3.8509959	0.000118	0.01187608
Zm00004b004118	GRMZM2G1674351	Zm00001d032728	(1 of 30) K15397 - :B4FQN3	3-ketoadyl-CoA syn	5.68148542	-5.9587649	1.39894683	-4.2594649	0.0000205	0.00273966
Zm00004b009098	GRMZM2G134351	Zm00001d005859	(1 of 1) PTHR1368:A0A1D6ERB3	Eukaryotic aspartyl	5.80723206	-5.9856396	1.47557762	-4.0564722	4.98E-05	5.94E-03
Zm00004b030863	GRMZM2G044457	Zm00001d038536	(1 of 3) PTHR1098:A0A1D6M733	Endoplasmic reticul	21.3259172	-6.0051667	1.52724447	-3.9320271	0.0000842	0.0091077
Zm00004b038273	GRMZM2G316593	Zm00001d023907		K7TJX6	Uncharacterized pr	6.29336864	-6.1070367	1.73815496	-3.5135168	0.0000442
Zm00004b040445	GRMZM2G007477	Zm00001d026489	(1 of 1663) 2.7.11.1 K7TP92	OSJNBb0022F16.1	39.149517	-6.3328095	1.31171634	-4.8278803	0.00000138	0.000268
Zm00004b006220	GRMZM2G114861	Zm00001d002186	(1 of 1) PTHR2411:A0A1D6DXK1	Kinesin-like protein	7.4353572	-6.3452997	1.54048688	-4.1190222	0.000038	0.00473499
Zm00004b039285	GRMZM2G081585	Zm00001d025106	(1 of 9) K04564 - s:K7U2E7	Superoxide dismut	7.93221065	-6.4429844	1.37152492	-4.6976794	0.00000263	0.0000473
Zm00004b000181	GRMZM2G176585	Zm00001d027447	(1 of 3) PTHR3187:A0A1D6JM71	Det1 complexing ut	67.4247474	-6.7039036	1.08801441	-6.1615945	7.20E-10	2.69E-07
Zm00004b034890	GRMZM2G107408	Zm00001d018906		B4FF39	Uncharacterized pr	200.726775	-6.8974602	1.62732124	-4.2385363	0.0000225
Zm00004b038011	GRMZM2G381429	Zm00001d023553	(1 of 2) PTHR2315:A0A1D6IU36	Disease resistance	14.1893652	-7.2758491	1.37114923	-5.3063875	0.000000112	0.000027
Zm00004b026342	GRMZM2G157705	Zm00001d010455		A0A1D6FR41	Reticulon-like prote	14.4386388	-7.3062458	1.43186922	-5.102593	0.000000335
Zm00004b038742	GRMZM2G148316	Zm00001d024476		A0A1D6IZI6	UDP-glycosyltransf	15.6056043	-7.4185534	1.49455082	-4.9637344	0.00000692
Zm00004b026136	GRMZM2G149808	Zm00001d010206	(1 of 3) PTHR1328:B4FT44	SAP30_Sin3_bdg d	16.0010348	-7.4530717	1.89630859	-3.9303553	8.48E-05	9.12E-03
Zm00004b013786	GRMZM2G137495	Zm00001d016440	(1 of 2) PTHR2407:A0A1D6H7L4	DNAJ heat shock fe	35.5552131	-7.6372363	1.23540564	-6.1819665	6.33E-10	2.46E-07
Zm00004b037949	GRMZM2G0839644	Zm00001d023470	(1 of 21) PF00560/A0A1D6ITF5	Putative leucine-ricl	19.8102521	-7.7609484	1.69935714	-4.5669908	0.00000495	0.0000283
Zm00004b001530	GRMZM2G134671	Zm00001d029149	(1 of 52) PF06203 - C0P33	C2C-CO-like trans	19.836807	-7.763756	1.7767038	-5.7682885	1.24E-05	1.76E-03
Zm00004b039025	GRMZM2G016312	Zm00001d024798		K7TM15	Uncharacterized pr	19.9227091	-7.7693616	2.19202511	-3.5443762	0.000394
Zm00004b017703	GRMZM2G0813403	Zm00001d042016	(1 of 309) 6.3.2.19 - B6TIZ5	Uncharacterized pr	20.0343	-7.7752321	1.58789062	-4.8965791	0.000000975	0.000193
Zm00004b005561	GRMZM2G347056	Zm00001d034602	(1 of 1) K00297 - m A0A1D6L979	Brown midrib2	21.7107574	-7.8927693	1.98910339	-3.9680035	7.25E-05	0.0081949
Zm00004b031719	GRMZM2G455243	Zm00001d045080	(1 of 2) K02603 - or A0A1D6NTH3	Origin recognition c	24.1413339	-8.0473034	1.29821421	-6.1987485	5.69E-10	0.00000023
Zm00004b001743	GRMZM2G018771	Zm00001d022337	(1 of 2) 3.5.1.88 - P.A0A1D6IL69	Peptide deformylas	25.1511161	-8.1065104	1.405358	-5.7682885	8.01E-09	2.30E-06
Zm00004b022114	GRMZM2G418604	Zm00001d051183	(1 of 1) K14327 - re A0A1D6Q5H4	Regulator of nonsei	25.6683286	-8.1347867	1.87357723	-4.3418476	0.0000141	0.00194146
Zm00004b018825	GRMZM2G093101	Zm00001d043291	(1 of 1) PTHR2295:A0A1D6NA73	Purple acid phosph	29.2236183	-8.3224876	1.26522035	-6.5778958	4.77E-11	2.25E-08
Zm00004b007010	GRMZM2G086486	Zm00001d003117	(1 of 3) PTHR1074:A0A1D6E6T4	40S ribosomal prote	29.5062216	-8.3337836	1.31279641	-6.3481157	2.18E-10	9.58E-08
Zm00004b005777	GRMZM2G164547	Zm00001d034859		B7ZZ71	Cobalt ion binding	30.292121	-8.3727734	2.14441788	-3.9044504	0.0000944
Zm00004b021733	GRMZM2G059803	Zm00001d042049	(1 of 3) 1.6.99.1 - N.A0A1D6N0R1	Ferredoxin-NADP I	34.0645512	-8.4011245	1.56595333	-5.3648626	0.000000881	0.0000203
Zm00004b005843	GRMZM2G077222	Zm00001d034935	(1 of 2) K0G3251 - A0A1D6LCC1	Uncharacterized pr	37.6670904	-8.6870873	1.69872918	-5.1138742	0.000000316	0.000071
Zm00004b019700	GRMZM2G070961	Zm00001d044293	(1 of 4) PF00069/P.A0A1D6NKI4	Protein kinase prote	38.4859778	-8.716857	1.32060373	-6.6006606	4.09E-11	1.98E-08
Zm00004b031672	GRMZM2G447806	Zm00001d045009		A0A1D6NST3	Uncharacterized pr	42.7021894	-8.8681762	1.51122296	-5.8682116	4.41E-09
Zm00004b000867	GRMZM2G043584	Zm00001d028317	(1 of 34) PF00069/A0A1D6JUB4	Leucine-rich repeat	50.3398948	-9.1050678	1.62156852	-5.6149757	1.97E-08	5.26E-06
Zm00004b020252	GRMZM2G468280	Zm00001d048796	(1 of 3) PTHR2276:A0A1D6P059	RING/U-box superf	53.9469078	-9.2054014	2.53250159	-6.3439405	2.78E-04	2.34E-02
Zm00004b015124	GRMZM2G036418	Zm00001d018057	(1 of 1) PTHR1352:A0A1D6HKI4	RINT1-like protein \uparrow	55.1481017	-9.2386971	1.2420628	-7.4381884	1.02E-13	8.08E-11
Zm00004b003465	AC234528_1_FG00	Zm00001d031928	(1 of 1) PF11595 - FB6TZS4	Uncharacterized pr	60.0901134	-9.3602792	1.25718448	-7.4454301	9.66E-14	7.97E-11
Zm00004b003059	GRMZM2G0881803	Zm00001d038205	(1 of 4) PTHR3194:A0A1D6M4I8	MLO-like protein	77.0738763	-9.7205791	1.63722392	-5.9372325	2.90E-09	9.89E-07
Zm00004b008558	GRMZM2G114220	Zm00001d002598	(1 of 1) PTHR1255:B6T4L6	Ubiquitin fusion deg	82.6579962	-9.8207032	1.42068652	-6.9126462	4.76E-12	2.69E-09
Zm00004b012058	GRMZM2G366638	Zm00001d0114207		A0A1D6GR10	Uncharacterized pr	85.6508137	-9.8719883	1.23584383	-7.9880549	1.37E-15
Zm00004b024150	GRMZM2G171452	Zm00001d053625	(1 of 21) PF01918 - B6T175	Alba DNA/RNA-bin	93.8008006	-10.004327	1.24530628	-8.0336274	9.46E-16	1.01E-12
Zm00004b031781	GRMZM2G023636	Zm00001d045147	(1 of 2) PTHR1893:A0A1D6NU12	Putative pre-mRNA	99.6267326	-10.090917	2.06077138	-4.8966967	0.000000975	0.000193
Zm00004b031625	GRMZM2G088053	Zm00001d044951	(1 of 54) PF00892 - B4FTK8	WAT1-related prote	124.401544	-10.411613	1.27855043	-8.1432945	3.85E-16	5.07E-13
Zm00004b024037	GRMZM2G029058	Zm00001d053452	(1 of 5) PF00076/P.A0A1D6QP55	Polyadenylate-bindi	203.284528	-11.119527	1.67867824	-6.6239776	3.50E-11	1.77E-08
Zm00004b003203	GRMZM2G386209	Zm00001d031555	(1 of 8) K0G4293 - A0A1D6KJM6	Cytochrome b561 a	221.282815	-11.242145	1.39757195	-8.0440548	8.69E-16	1.01E-12
Zm00004b007229	GRMZM2G029001	Zm00001d003394	(1 of 7) PTHR1260:A0A1D6E920	RING/U-box superf.	221.630087	-11.244202	1.92064065	-5.8544018	4.79E-09	0.00000146
Zm00004b030622	GRMZM2G175676	Zm00001d038248	(1 of 4) K12831 - s: A0A1D6M4R6	RNA-binding (RRM	322.560854	-11.785783	1.82352341	-6.4631924	1.03E-10	4.61E-08
Zm00004b018149	GRMZM2G064914	Zm00001d042512	(1 of 2) PTHR1124:A0A1D6N4Q6	Ribonuclease 2	421.632858	-12.171961	3.56098798	-3.4181417	0.000631	0.04536639
Zm00004b011884	GRMZM2G114557	Zm00001d013195	(1 of 3) PTHR1238:A0A1D6GGF2	Thylakoidal proces	443.480025	-12.24485	3.58774162	-3.4129687	0.000643	0.04573738
Zm00004b019678	GRMZM2G084896	Zm00001d044267	(1 of 2) K18121 - gl A0A1D6NK13	Glyoxylate/succinic	469.510211	-12.327109	1.22910896	-10.029306	1.13E-23	3.20E-20
Zm00004b037198	GRMZM2G167932	Zm00001d021999	(1 of 1) PF02136/P.A0A1D6IIC4	Nuclear transport fa	497.082753	-12.409565	1.38506885	-8.9595291	3.26E-19	4.96E-16
Zm00004b019828	GRMZM2G143128	Zm00001d044445	(1 of 2) K03661 - V-#N/A	#N/A	507.068603	-12.438167	3.57743815	-3.4786365	0.000507	0.03801417
Zm00004b003707	GRMZM2G092595	Zm00001d032238	(1 of 1) PTHR1135:A0A1D6KPG0	Putative 1-phospha	598.995823	-12.678531	3.6072989	-3.5146883	0.00044	0.03378431
Zm00004b037850	GRMZM2G129804	Zm00001d023340	(1 of 1) K02356 - ei A0A1D6ISX4	Elongation factor P	830.618221	-13.150242	1.20932357	-10.874048	1.53E-27	1.01E-23
Zm00004b031504	GRMZM2G026833	Zm00001d044785	(1 of 334) PF00249 K7W4V3	G2-like1	1385.73578	-13.888696	1.34835579	-10.300468	7.01E-25	2.77E-21
Zm00004b026230	GRMZM2G086464	Zm00001d010314		A0A1D6FQC3	Uncharacterized pr	1530.26023	-14.031661	3.71963824	-3.7723187	1.62E-04
Zm00004b000190	GRMZM2G177508	Zm00001d027456	(1 of 3) PTHR3322:B4FTJ9	PBA1 homolog1 (Tl	9043.16785	-16.594887	1.31130707	-12.655226	1.05E-36	2.07E-32

TABLE NOTES:

... GENEIDs B73v3 GeneIDs were obtained from the W22 GeneIDs using a MaizeGDB syntelogs lookup table made with SynMap
 ... E: Trimmed reads were aligned using the splice-aware aligner Hisat2, indices were constructed from known exons and splice sites (W22 annotation Zm00004b & assembly Zm-W22-REFERENCE-NRGENE-2.0 as describe
 TABULATION: Differential expression analysis was performed separately per tissue (leaf mutant vs. WT or tassell mutant vs. WT) as described in the Methods
 TABULATION: This entire table, sorted on col-H, log2(fold-change), includes statistically significant differentially expressed (adjusted p-value <0.05) genes and excludes any genes with fewer than 10 counts across sum of all replicates.
 COLUMNS G-L: Columns G-L tabulate output values for the baseMean, the log2(fold-change), along with the associated values for standard error (lfcSE), Wald statistic (stat), pvalue, and adjusted pvalue (padj).
 PROVENANCE: Supplementary Table S2 from McKenna, Gumber, et al., "Maize (Zea mays L.) nucleoskeletal proteins regulate nuclear envelope remodeling...", submitted 12/2020, FIPS

Table S2: Differentially expressed genes between *mkaku1* mutant versus wildtype plants for maize leaf and tassel.

Table S2 (Tab 2 of 2) TASSEL DEGs. All 155 Differentially Expressed Genes from Tassel.

W22v2 GeneID	B73v3 GeneID	B73v4 GeneID	Phytomine description	Uniprot id	Uniprot descriptor	baseMean-LEAF	log2FoldChange (mutant/wt)	fcSE	stat	pvalue	padj
Zm00004b019058	GRMZM2G031308	Zm00001d043551	(1 of 5) PTHR1099:B6TGL5		Reticulon-like prote	1116.51594	13.6331752	3.54537242	3.84534362	0.00012	0.01847303
Zm00004b0371958	GRMZM2G167932	Zm00001d021999	(1 of 1) PF02136/F/AA01D6IIC4		Nuclear transport fe	927.603007	13.3657652	3.51855276	3.79865296	0.000145	0.02157566
Zm00004b040337	GRMZM2G097854	Zm00001d026369	(1 of 3) K08695 - arAA01D6JF45		Anthocyanidin redu	832.100873	13.2090143	3.56596764	3.70418794	0.000212	0.02892647
Zm00004b016461	GRMZM2G091119	Zm00001d040274	(1 of 4) PF00514/F/AA01D6MPN9		Importin subunit alp	766.55018	13.0909203	1.25615948	10.4296725	1.82E-25	6.68E-22
Zm00004b012240	GRMZM2G085967	Zm00001d014467	(1 of 1) PTHR3123:B6THU9		Peroxidase (EC 1.1	759.921198	13.0781172	3.49760919	3.7391591	0.000185	0.02582228
Zm00004b030603	GRMZM2G016817	Zm00001d038208	(1 of 4) PTHR1232:B6TK34		PHD finger protein	677.775636	12.9132908	1.50630854	8.5728059	1.01E-17	1.49E-14
Zm00004b012451	GRMZM2G084521	Zm00001d014732	(1 of 1) PTHR1107:AA01D6GVX5		Peptidyl-prolyl cis-t	477.323952	12.4072467	3.43872232	3.60809788	0.000308	0.03962687
Zm00004b034468	GRMZM2G063060	Zm00001d048409	(1 of 5) K13525 - trAA01D6PJ20		Cell division control	651.478524	11.8939283	2.18052918	5.45460636	4.91E-08	0.0000155
Zm00004b031400	GRMZM2G099529	Zm00001d039167	(1 of 1) PTHR1038:B4F9Z4		ATP-dependent Clp	315.8768	11.8117851	1.25206243	9.4338627	3.95E-21	7.94E-18
Zm00004b022426	GRMZM2G147701	Zm00001d051552	(1 of 2) 1.1.1.102 - :K7U3E5		3-dehydroshpingan	287.984997	11.6784178	1.54025663	7.58212465	3.40E-14	2.89E-11
Zm00004b003468	GRMZM2G103258	Zm00001d031933	(1 of 2) K09598 - siB6T57		Signal peptide pept	170.324314	10.9206558	1.90401389	5.73559672	9.72E-09	0.00000352
Zm00004b002034	GRMZM2G453832	Zm00001d029808	(1 of 3) PTHR1389:AA01D6K7V9		Magnesium transp	153.353766	10.7689598	1.36515021	7.88847976	3.06E-15	3.56E-12
Zm00004b014513	GRMZM2G169967	Zm00001d017377	(1 of 8) PF01357//AA01D6HEG4		Beta-expansin 3	145.470907	10.6932269	1.51068068	7.07841642	1.46E-12	9.21E-10
Zm00004b006032	GRMZM2G061745	Zm00001d001966	(1 of 2) K03038 - 2fAA01D6DUX4		26S proteasome cn	141.170616	10.649926	1.29679144	8.21252027	2.17E-16	2.99E-13
Zm00004b013432	GRMZM2G130425	Zm00001d016034	(1 of 2) K03363 - ceCOP1V0		Cell-division cycl	52.9193026	10.275466	2.88710491	9.0058994	0.000372	0.04619789
Zm00004b032186	GRMZM2G459172	Zm00001d045615	(1 of 2) PTHR1266:AA01D6NKR5		Protein FATTY ACIL	86.95675	9.95034834	1.28432357	7.74754008	9.37E-15	9.10E-12
Zm00004b036844	GRMZM2G822284	Zm00001d021072	(1 of 3) PF13889 - (AA01D6I880		DUF4210 domain-c	83.2929674	9.88888472	1.23694461	7.99460599	1.30E-15	1.60E-12
Zm00004b025017	GRMZM2G032190	Zm00001d008759			Copper ion binding	70.5856734	9.64930986	1.60646012	6.0056667	1.89E-09	7.48E-07
Zm00004b001099	GRMZM2G100086	Zm00001d028585	(1 of 4) PTHR3060:AA0A96RK86		RNA polymerase sII	49.6978463	9.14362243	1.26003287	7.25665535	3.97E-13	2.74E-10
Zm00004b012918	GRMZM2G170805	Zm00001d014692	(1 of 4) PF06094 - (B4FVZ7		AlG2-like protein	266.67295	9.1671684	9.00708367	1.0505799	9.13E-24	2.52E-20
Zm00004b004132	GRMZM2G134747	Zm00001d032736	(1 of 1) 4.2.1.104 - (AA01R3MBN3		Cyanate hydratase	338.974496	8.80622145	2.35087671	3.74593079	0.00018	0.02545775
Zm00004b037937	GRMZM2G148404	Zm00001d023453			Uncharacterized pr	37.7204071	8.74631485	1.56432485	5.5911163	2.26E-08	0.00000755
Zm00004b023615	GRMZM2G397281	Zm00001d052963			EGF-like domain-cc	34.783636	8.6294773	1.42645668	6.04958947	1.45E-09	6.05E-07
Zm00004b039332	GRMZM2G139407	Zm00001d025165	(1 of 4) PTHR1069:K7TNM4		Nuclear transport fa	342.380841	8.38816455	1.93661663	4.33135004	0.000148	0.00287999
Zm00004b013393	GRMZM2G019553	Zm00001d015988	(1 of 1) K02200 - cyB6SU73		Cytochrome c-type	27.3880869	8.28329824	2.02586486	4.08877137	0.0000434	0.00772796
Zm00004b027287	GRMZM2G030284	Zm00001d011615	(1 of 13) K16732 - fB4F8V2		65-kDa microtubule	167.362819	7.92131804	6.02039446	9.9592287	0.000762	0.01266669
Zm00004b032576	GRMZM2G083841	Zm00001d046170	(1 of 3) PTHR3052:Q43267		PEP carboxylase (F	18.6138473	7.72779073	1.43542165	5.38363813	7.30E-08	0.0000218
Zm00004b040223	GRMZM2G415229	Zm00001d026245	(1 of 6) PTHR1003:AA01D6JDK2		Trithelix transcrip	18.1600557	7.69219139	1.58572195	4.85098005	0.0000123	0.000289
Zm00004b036145	GRMZM2G127537	Zm00001d020670	(1 of 2) PF00046/F/B4F59		HB transcription fac	17.7078164	7.65622705	1.41089273	5.42651252	5.75E-08	0.0001799
Zm00004b018381	GRMZM2G831584	Zm00001d042762	(1 of 2) 3.1.1.89 - PAA01D6N6L2		Catalytic/ hydrolase	64.6504735	7.56126644	1.36363639	5.54492049	2.94E-08	0.0000097
Zm00004b039799	GRMZM2G005939	Zm00001d025752			Transcription factor	83.7504033	7.52422242	1.202317	6.6810199	3.90E-10	1.83E-07
Zm00004b011538	GRMZM2G822180	Zm00001d013598	(1 of 6) PF14368 - B4G0Q2		Lipid binding protei	30.572681	7.48199367	1.31879864	5.67334044	1.40E-08	0.00000491
Zm00004b028398	GRMZM2G032315	Zm00001d035087	(1 of 3) K02942 - laB6T361		60S acidic ribosom	9.95098821	6.76511433	1.79409873	3.77075922	0.000163	0.02340051
Zm00004b039943	GRMZM2G017815	Zm00001d025911	(1 of 11) PTHR142:K7U5C2		Transducin/WD40 r	62.494728	6.76470472	1.9033603	3.55408523	0.000379	0.04654892
Zm00004b019310	GRMZM2G316223	Zm00001d043819	(1 of 1) PF00415/F/AA01D6NF99		Uncharacterized pr	9.45026789	6.74829124	1.45030119	4.65302745	0.00000327	0.00073
Zm00004b005589	GRMZM2G155329	Zm00001d034635	(1 of 1) K01859 - ctB6TJA9		Chalcone- flavonone	2498.54833	6.712817	1.6798008	3.99619824	0.0000644	0.01094105
Zm00004b018181	GRMZM2G328795	Zm00001d042558	(1 of 1) PTHR3179:AA01D6N567		TPR repeat-contain	8.74339242	6.63790001	1.75838949	3.77498844	0.00016	0.02340051
Zm00004b037112	GRMZM2G092669	Zm00001d021879	(1 of 11) PF14365 - B4G0L1		NEP-interacting pr	449.338405	6.52571887	1.54959928	4.21122992	0.0000254	0.00479683
Zm00004b027462	GRMZM2G167758	Zm00001d011799	(1 of 1) PTHR3421:K7V1E4		Nuclear transport fe	7.40410104	6.39553672	1.61471115	3.96079307	0.0000747	0.0125051
Zm00004b009299	GRMZM2G179002	Zm00001d006102	(1 of 4) PTHR2288:AA01D6ESW0		40S ribosomal prot	355.743669	6.22902942	0.6923039	8.99753627	2.31E-19	3.92E-16
Zm00004b026474	GRMZM2G827266	Zm00001d010614	(1 of 3) K02976 - srAA01D6FSC6		Uncharacterized pr	43.1226968	6.11457177	1.01798407	6.00654957	1.90E-09	7.48E-07
Zm00004b014767	GRMZM2G428233	Zm00001d017658	(1 of 11) PF08458 - AA01D6HG97		Uncharacterized pr	5.23476558	5.8965248	1.65059434	3.5723646	0.000354	0.04467034
Zm00004b033022	GRMZM2G180863	Zm00001d046742	(1 of 1) PTHR1021:B7ZZ73		Ribose-phosphate j	199.077229	5.86648046	1.33522799	4.39361704	0.0000111	0.00223943
Zm00004b008843	GRMZM2G346865	Zm00001d005544	(1 of 2) PTHR1931:AA01D6ENR8		ARM repeat superf	46.3742592	5.855099	1.26125486	6.44228063	0.0000345	0.000761
Zm00004b026907	AC207342_3_F000	Zm00001d011145	(1 of 3) PF13474 - (B4FETO		F-box protein SKIPI	66.4771194	5.81106553	1.48313606	3.91809333	0.0008993	0.01429134
Zm00004b025652	GRMZM2G058913	Zm00001d009591	(1 of 4) PTHR1275:AA01D6FKE6		GBF-interacting pr	72.2310448	5.80719248	1.51786221	3.82590228	0.00013	0.01958575
Zm00004b017977	GRMZM2G119650	Zm00001d042309	(1 of 2) PTHR3213:AA01D6N2R0		F-box only protein f	190.959684	5.45833106	1.22510187	4.45540997	0.0000837	0.00174552
Zm00004b033705	GRMZM2G462803	Zm00001d047540	(1 of 1) PF06920//AA01D6PBF4		Guanine nucleotide	134.054619	5.44016169	1.23490804	4.40531726	0.0000106	0.00216119
Zm00004b014532	GRMZM2G068340	Zm00001d017392	(1 of 2) PTHR1002:AA01D6HEM4		Cyclin-T1-3	198.893809	5.38931983	1.45077883	3.71477699	0.000203	0.02798318
Zm00004b018190	GRMZM2G070562	Zm00001d042659	(1 of 1) K03108 - siAA01D6N584		Signal recognition f	71.7560358	5.37996285	0.62550463	8.60099611	7.90E-18	1.25E-14
Zm00004b025991	GRMZM2G102745	Zm00001d010203	(1 of 2) K15115 - scAA01D6FNM8		Nicotinamide adenin	56.4004262	4.96359461	1.39255218	3.5643868	0.000365	0.04578948
Zm00004b034487	GRMZM2G115674	Zm00001d048431	(1 of 3) PF15365 - IK7VQD7		Uncharacterized pr	96.1690586	4.93403936	1.29122851	3.82119766	0.000133	0.01982835
Zm00004b015186	GRMZM2G072300	Zm00001d018131	(1 of 173) PTHR24(AA0A96R205		Chaperone protein	21.6294645	4.72947748	1.13382031	4.17127603	0.0000303	0.0056245
Zm00004b032905	GRMZM2G105167	Zm00001d046592	(1 of 2) K0G3306 - K7VV99		ER membrane prot	206.287168	4.7121818	1.15860049	4.07490058	0.000046	0.00813771
Zm00004b030094	GRMZM2G034622	Zm00001d037557	(1 of 1) K10589 - utAA01D6LYY6		E3 ubiquitin-protein	519.15557	4.71657044	0.80201653	5.88088928	4.08E-09	0.00000155
Zm00004b030898	GRMZM2G020150	Zm00001d038855	(1 of 213) PF00847:AA01D6MD71		Putative F52/EREB	56.826908	4.70792367	0.73702313	6.38775662	1.68E-10	8.09E-08
Zm00004b021954	GRMZM2G006672	Zm00001d050965	(1 of 5) K00030 - isAA01D6Q461		Isocitrate dehydrog	16.045869	4.53410659	1.20156413	3.77350362	0.000161	0.02340051
Zm00004b028599	GRMZM2G036908	Zm00001d035447	(1 of 3) K14689 - scAA01D6LGF5		Metal tolerance pro	409.16687	4.46231855	0.59555026	7.49276567	6.74E-14	5.32E-11
Zm00004b012681	GRMZM2G080638	Zm00001d014998	(1 of 1) PTHR1398:COPP15		FACT complex subu	1291.20935	4.46041724	0.58607138	7.61070651	2.73E-14	2.41E-11
Zm00004b034033	GRMZM2G101001	Zm00001d047912			COPB4	472.429917	4.30781299	1.1409786	3.77554232	0.00016	0.02340051
Zm00004b023245	GRMZM2G059381	Zm00001d052485	(1 of 2) PTHR2409:B6SWE6		AMP-binding protei	239.813652	4.19842567	1.15390827	3.6384397	0.000274	0.00586466
Zm00004b033266	GRMZM2G116327	Zm00001d047063	(1 of 2) PTHR2825:B6SKI7		Camphor resistanc	230.168414	4.14211418	0.70868349	5.84480126	5.07E-09	0.00000187
Zm00004											

Zm00004b037183	GRMZM2G411916	Zm00001d021972	(1 of 7) K01530 - pt:AOA1D6I179	Elongation-transf	599.743563	0.91273641	0.17158889	5.31932126	1.04E-07	0.000291
Zm00004b005747	GRMZM2G056393	Zm00001d034826	(1 of 1) PTHR2311:AOA1D6LBQ9	Phospholipid factor G	962.317187	0.88687693	0.24287944	3.65151094	0.000261	0.03491353
Zm00004b005063	GRMZM2G033135	Zm00001d033935	(1 of 2) K08873 - P1AOA1D6L3E8	Serine/threonine-pr	905.356031	0.8536198	0.23391793	3.64922778	0.000263	0.03496643
Zm00004b018233	GRMZM2G034639	Zm00001d042615	(1 of 1) PF08729 - IAOA1D6N5F5	Wound-responsive	762.996245	0.68630198	0.15886115	4.32013723	0.0000156	0.00302249
Zm00004b025122	GRMZM2G472625	Zm00001d008893	(1 of 2) PTHR2405:B4FE45	Shaggy-related pro	1487.53332	0.67939668	0.14209803	5.47467734	4.38E-08	0.0000142
Zm00004b038192	GRMZM2G331368	Zm00001d023795	(1 of 3) K10592 - E:AOA1D6IVN3	E3 ubiquitin-protein	4755.10766	0.65216734	0.15818723	4.12275591	0.0000374	0.00678063
Zm00004b022902	GRMZM2G449909	Zm00001d052110	(1 of 1) PTHR1314:AOA1D6QDE1	Opaque endosperr	1134.47856	0.55751927	0.14787332	3.77024932	0.000163	0.02340051
Zm00004b020700	GRMZM2G026459	Zm00001d049349	(1 of 2) PTHR1165:AOA1D6PTX6	Protein NRT1/ PTR	791.740497	-0.6716858	0.16230397	-4.1384435	0.000035	0.00638567
Zm00004b011043	GRMZM2G115612	Zm00001d013046	(1 of 3) PTHR1496:AOA1D6GF85	Lipid phosphate ph	714.795212	-0.8131227	0.20154562	-0.0344349	0.0000547	0.00952326
Zm00004b017318	GRMZM2G098397	Zm00001d041511	(1 of 5) K07964 - h:AOA1D6MWN0	Heparanase-like pr	763.079646	-0.9465329	0.22192695	-4.2650651	0.00002	0.00380686
Zm00004b022535	GRMZM2G012814	Zm00001d051687	(1 of 2) PTHR1098:K7U856	Rho GDP-dissociat	102.730112	-1.3999356	0.36476726	-3.8378871	0.000124	0.0189116
Zm00004b020861	GRMZM5G870572	Zm00001d049563	(1 of 1) K03141 - tr:AOA1D6PW70	Putative RNA polyr	249.64317	-1.6236128	0.22531901	-7.2058404	5.77E-13	3.86E-10
Zm00004b033123	GRMZM2G058162	ubiquitin-conjugatin	(1 of 3) PTHR2406:#N/A	#N/A	690.415242	-2.0449529	0.37385177	-5.4699566	4.50E-08	0.0000144
Zm00004b000914	GRMZM2G157177	Zm00001d028372	(1 of 4) PTHR2295:AOA1D6JV15	BZIP transcription f.	71.0752415	-2.0593793	0.30429553	-6.7676948	1.31E-11	7.81E-09
Zm00004b030613	GRMZM2G153075	Zm00001d038224	(1 of 2) K03875 - F-B4FT72	F-box protein FBL2	218.253808	-2.0984351	0.57522464	-3.6480027	0.000264	0.03496643
Zm00004b034784	GRMZM2G012031	Zm00001d018795	(1 of 1) PTHR2436:AOA1D6HSC5	187-kDa microtubul	1281.82697	-2.5686201	0.38603854	-6.6537919	2.86E-11	1.62E-08
Zm00004b029454	GRMZM5G829955	Zm00001d036709	(1 of 1) K12857 - P1AOA1D6LQJ4	Transducin/WD40 r	72.5753958	-2.5762318	0.34823181	-7.398037	1.38E-13	9.85E-11
Zm00004b007383	GRMZM2G371721	Zm00001d022168	(1 of 5) PTHR2407:QSGAN9	AT hook-containing	66.8457668	-2.7007364	0.36102147	-7.4808194	7.39E-14	5.63E-11
Zm00004b011381	GRMZM2G090172	Zm00001d013431	(1 of 2) PTHR2406:AOA1D6GJ80	Ubiquitin-conjugatir	178.729135	-2.7762387	0.68518628	-4.0518014	0.0000508	0.0089133
Zm00004b016600	GRMZM2G305264	Zm00001d040445	(1 of 2) PTHR2276: COPF84	RING/U-box superi.	134.364196	-3.1863228	0.66813468	-4.7689828	0.0000185	0.000426
Zm00004b005951	GRMZM2G040115	Zm00001d001858	(1 of 45) PF03000 - BBA094	Thioredoxin domain-c	95.666743	-3.2570704	0.84535642	-3.852896	0.000117	0.01803748
Zm00004b006866	GRMZM2G176677	Zm00001d002945	(1 of 151) PF02365 AOA1D6E5L0	Ras-related protein	359.948291	-3.3304859	0.61989729	-5.3726415	7.76E-08	0.0000227
Zm00004b007383	AC235541.1_FG00	Zm00001d003948	(1 of 3) PTHR2407:CAJ193	DNAJ heat shock N	109.280361	-2.4489189	0.09709931	-3.5519273	0.000382	0.04654892
Zm00004b032487	GRMZM2G057743	Zm00001d046033	(1 of 2) PTHR1028:K7W8X7	RNA-binding KH do	35.6783799	-3.4498949	0.56344471	-6.1226361	9.19E-10	3.98E-07
Zm00004b030589	GRMZM2G133021	Zm00001d038194	(1 of 127) PF00646 COPeL8	F-box/FBD/LRR-rep	212.536727	-3.4882886	0.6674719	-5.2261206	1.73E-07	0.0000461
Zm00004b019813	GRMZM2G0812270	Zm00001d044429	(1 of 44) 5.3.4.1 - P-B6TH36	Thioredoxin superfe	158.728386	-3.5236272	0.97410544	-3.6172955	0.000298	0.03846912
Zm00004b001427	GRMZM2G312661	Zm00001d029028	(1 of 2) PTHR1089: COP445	Calcium-binding pr	49.7443658	-3.5317195	0.67313631	-5.2466631	1.55E-07	0.0000417
Zm00004b000119	GRMZM2G087600	Zm00001d028612	AOA1D6JY27	Uncharacterized pr	255.883023	-3.5347045	0.67840253	-5.210335	1.88E-07	0.000049
Zm00004b034015	GRMZM2G013814	Zm00001d047894	(1 of 7) PF11833 - FB6TKC3	Protein CHAPERON	119.776564	-3.546751	0.54232152	-6.5399414	6.15E-11	3.32E-08
Zm00004b037413	GRMZM2G180568	Zm00001d022256	(1 of 46) PF03634 - AOA060CZ25	TCP transcription fe	126.838844	-4.1765009	0.41628918	-10.032691	1.09E-23	2.69E-20
Zm00004b014162	GRMZM2G075637	Zm00001d016935	(1 of 2) K11290 - lei:Q94F78	Nucleosome/chrom	154.018655	-4.3893148	0.65387115	-6.712813	1.91E-11	1.11E-08
Zm00004b031562	GRMZM2G058560	Zm00001d044866	(1 of 1) K17605 - se:AOA1D6NRY3	Serine/threonine-pr	158.722343	-4.6022265	0.85675423	-5.3716998	7.80E-08	0.0000227
Zm00004b013626	GRMZM2G152328	Zm00001d013410	(1 of 2) PTHR11933:#N/A	#N/A	1408.63065	-4.8578728	0.62713761	-7.7461035	9.48E-15	9.10E-12
Zm00004b005296	GRMZM2G170727	Zm00001d034254	(1 of 3) KOG3381 - AOA1D6L6F1	Protein AE7-like 1	88.6494724	-5.7478947	1.45627857	-3.9469747	0.0000791	0.01305123
Zm00004b000303	GRMZM2G090914	Zm00001d027588	AOA1D6JN74	Uncharacterized pr	47.4651127	-6.0922781	1.65823335	-3.6739571	0.000239	0.03217847
Zm00004b036142	GRMZM2G0832772	Zm00001d020666	(1 of 58) 3.6.3.44 - :AOA1D6IK5K	Multidrug resistanc	85.8989549	-6.1529098	1.1384309	-5.4042004	6.51E-08	0.00002
Zm00004b040245	GRMZM2G018462	Zm00001d026259	(1 of 2) PTHR3397:AOA1D6JDS9	Uncharacterized pr	69.2136647	-6.6238048	1.70248072	-3.8906783	0.0001	0.01577795
Zm00004b039476	GRMZM2G095826	Zm00001d025352	(1 of 2) PTHR1937:B4FYW4	Ferredoxin	163.683221	-6.6902767	0.64379504	-10.391936	2.70E-25	8.52E-22
Zm00004b038507	GRMZM2G094452	Zm00001d024212	(1 of 7) K00901 - di:A8QM11	diacylglycerol kinas	14.1787349	-7.2001486	1.36678595	-5.2679417	1.38E-07	0.0000376
Zm00004b013692	GRMZM2G029559	Zm00001d016358	(1 of 1) PF00043/P:AOA1D6H6X9	Putative elongation	528.862948	-7.3168313	1.9781414	-3.6988414	0.000217	0.02936134
Zm00004b003529	GRMZM2G084853	Zm00001d032024	(1 of 2) PTHR1064:AOA1D6KN59	Myb transcription fa	15.7016476	-7.351001	1.59883256	-5.977298	0.0000427	0.000925
Zm00004b032897	GRMZM5G805627	Zm00001d046583	(1 of 5) K02955 - sr:AOA1D6P3R8	40S ribosomal prot	2049.55018	-7.3664354	1.37568503	-5.3547398	8.57E-08	0.0000243
Zm00004b004185	GRMZM2G144782	Zm00001d032810	(1 of 1) PTHR2131:AOA1D6KU49	CHY-type/CTCHY- γ	16.6392848	-7.4346907	1.64434719	-4.5213631	0.0000614	0.00130548
Zm00004b017739	GRMZM2G162250	Zm00001d042055	(1 of 3) PTHR3132:AOA1D6N0T2	ARGOS6	18.9738992	-7.6208123	1.68744911	-5.611731	0.000063	0.00132513
Zm00004b011561	GRMZM2G038801	Zm00001d013639	(1 of 2) PTHR1585:AOA1D6GL71	DnaJ/Hsp40 cystein	19.1338892	-7.6335474	2.14431334	-3.5590929	0.000371	0.04619789
Zm00004b013627	GRMZM2G121309	Zm00001d016277	(1 of 32) K14484 - :AOA1D6H6I5	Auxin-responsive pr	20.9605007	-7.7652893	2.16172134	-5.9217837	0.000328	0.04818081
Zm00004b039120	GRMZM2G174671	Zm00001d024908	(1 of 1) K01476 - ar:AOA1D6J2P7	Arginase 1 mitocho	124.634851	-7.8105926	2.01527474	-3.8756962	0.000106	0.01666212
Zm00004b038454	GRMZM2G062585	Zm00001d024155	(1 of 2) 3.1.3.21 - GB4FM45	(DL)-glycerol-3-pho	22.77030084	-7.8802551	1.29576777	-6.0815335	1.19E-09	5.06E-07
Zm00004b007737	GRMZM2G027272	Zm00001d004022	(1 of 3) K13456 - ri:AOA1D6ED15	RPM1-interacting p	95.7103695	-7.9584404	2.12649259	-3.7425197	0.000182	0.02564156
Zm00004b033732	GRMZM5G872256	Zm00001d047582	(1 of 3) 2.4.1.123 - I:Q7XYX1	Hexosyltransferase	31.5946066	-8.3574989	1.55936046	-5.3956683	8.34E-08	0.0000239
Zm00004b015097	GRMZM2G028325	Zm00001d018037	(1 of 5) PTHR1913:AOA1Q1ADS4	NOD26-like membr	37.5124823	-8.6059927	1.76417839	-4.8781873	0.0000107	0.000257
Zm00004b029343	GRMZM2G126920	Zm00001d000360	#N/A	#N/A	48.7785425	-8.9851403	1.817047	-4.9449135	7.62E-07	0.000185
Zm00004b018250	GRMZM2G135743	Zm00001d042627	(1 of 8) 2.4.1.17 - G:AOA1D6N5J7	Hexosyltransferase	982.742606	-9.016643	0.77835005	-11.584033	4.95E-31	5.47E-27
Zm00004b036596	GRMZM2G048165	Zm00001d021180	(1 of 1) PTHR2229:AOA1D6I9L5	Endoglyucanase (EC	50.8729068	-9.0456557	1.81462784	-9.9484545	0.0000062	0.000152
Zm00004b011870	GRMZM2G001887	Zm00001d013999	(1 of 5) K01527 - nr:AOA1D6GPC3	Basic transcription I	53.8848989	-9.1296606	1.47437162	-6.1922384	5.93E-10	2.67E-07
Zm00004b039616	GRMZM2G097499	Zm00001d025538	AOA1D6J7M0	Uncharacterized pr	61.4228893	-9.3179732	2.14512664	-4.343787	0.000014	0.00276306
Zm00004b003293	GRMZM2G452523	Zm00001d031691	(1 of 2) PF04055/P:AOA1D6KKQ0	Biotin synthase	122.070016	-9.3438471	1.50000812	-6.2291977	4.69E-10	2.16E-07
Zm00004b040319	GRMZM2G150950	Zm00001d026348	(M=2) PF02178 - A:K7TSL3	AT hook motif fami	66.1902783	-9.4249272	2.11675509	-4.4525355	0.00000849	0.00175252
Zm00004b000181	GRMZM2G176585	Zm00001d027447	(1 of 3) PTHR3187:AOA1D6JM71	Det1 complexing ut	66.744177	-9.4374569	2.07279808	-4.5530035	0.0000529	0.00113457
Zm00004b009722	GRMZM2G099239	Zm00001d006626	(1 of 32) PF03763 - AOA1D6EZ75	Remorin family prot	134.038381	-9.4798187	2.21758152	-4.2748456	0.0000191	0.00367521
Zm00004b031639	GRMZM2G142072	Zm00001d044971	(1 of 3) K15172 - tr:AOA1D6NSG9	Transcription elong:	85.8177719	-9.7999257	1.58831871	-6.1699996	6.83E-10	3.02E-07
Zm00004b036768	GRMZM2G131275	Zm00001d021489	(1 of 23) PF03759 - AOA1D6IBJ1	Rop guanine nucle	92.4669284	-9.9071476	1.42087283	-6.9725786	3.11E-12	1.91E-09
Zm00004b029791	GRMZM2G048194	Zm00001d037151	(1 of 3) PTHR2335:AOA1D6LUX5	Erwinia induced pr	503.899342	-9.9154886	0.93584643	-10.595209	3.14E-26	2.31E-22
Zm00004b015296	GRMZM2G095778	Zm00001d018278	(1 of 2) PTHR2803:B4F9M5	Fatty-acid-binding p	96.9447582	-9.9763143	1.54298423	-6.4655971	1.01E-10	5.19E-08
Zm00004b011028	AC210013.4_FG01	Zm00001d013030	(1 of 3) PTHR2434:B4FF99	Calcium-dependent	100.245209	-10.023864	1.99183346	-5.0324812	4.84E-07	0.00012
Zm00004b026211	GRMZM2G007384									

Figure S3: Multiple Seq Alignment of Transcripts.

Addgene gene ID	Plasmid name	Plasmid type	N-terminal Tag	Backbone Name	Bacterial Resistance
131014	MKAKU41ec	entry vector	mCherry-FLAG-HA	pDONR221	Kanamycin
131015	MKAKU41exp	expression vector	mCherry-FLAG-HA	pH7WG2	Spectinomycin
131016	NCH1ec	entry vector	eGFP-FLAG-HA	pDONR221	Kanamycin
131017	NCH1exp	expression vector	eGFP-FLAG-HA	pH7WG2	Streptomycin
131018	NCH2ec	entry vector	eGFP-FLAG-HA	pDONR221	Kanamycin
131019	NCH2exp	expression vector	eGFP-FLAG-HA	pH7WG2	Spectinomycin
159097	p35S::mCherry-GFP-HDEL	expression vector	mCherry-GFP	pB7FWG2	Spectinomycin

Supplementary Table S3 is from Mckenna, Gumber, et al.,

"Maize (*Zea mays* L.) nucleoskeletal proteins regulate nuclear envelope remodeling...", submitted 12/2020, FiPS